CHAPTER 3- Part 1

MATERIAL and METHODS

The specimens used in this study comprise extant and extinct dental material. The extant material derives from a previous study of Reid *et al.*; (1998a) on an archaeological medieval population and from ground sections specifically prepared for this study. The newly sectioned material derives from another archaeological population dating to the VII to VIII century in France, known as the Merovingian. The Reid *et al*.; (1998a) and Merovingian samples consist of ground sections of molars sectioned along the apices of the mesial or distal cusps (Tables 3.5-3.7). These were subsequently examined with incident and polarized light microscopy. The fossil material comprises naturally fractured teeth and four previously sectioned specimens prepared by Grine and Martin (1988) and housed at the hominid collections of the Transvaal Museum, Pretoria, South Africa; and the Dept. of Anatomy, University of the Witwatersrand Medical School, Johannesburg, South Africa. Fossil specimens showing natural fractures which were surveyed for this study from both fossil repositories is indicated in Table 3.8. After a preliminary observation of the specimens using a stereoscopic microscope and the PCSOM, subset of these specimens were selected for analysis because striae and cross striations could be observed on the fractured surface. These selected specimens are further detailed in Table 3.9.

SECTION 1: Methods

Chapter 3 has been divided in two parts. The first part describes the methodology employed in the analysis of fossil and modern teeth. In addition, a general description of the various components of the Portable Confocal Scanning Optical Microscope (PCSOM) are given, which are based on the work of Bromage *et al*.; (2003, 2005).

Chapter 8 includes further descriptions and more concise applications of this microscope to study fossil material. In the second part of Chapter 3, selected images which are most illustrative of enamel microstructural features when these are viewed with the PCSOM are shown. Differences in these features using different combinations of lenses, adapters and specimens with and without a clearing medium are also shown.

3.1. Microscopy used in this study

For the study of ground sections of *H. sapiens* and bonobo, a Zeiss Universal microscope with polarizing accessories and a Wild stereoscopic microscope were used. A white light source, usually orientated at low angles to the specimen, was used with the Wild microscope. A Nikon Coolpix 4500 digital camera was used to image the specimens and from these images, the angles striae/EDJ were measured using ImageJ software.

To image fossil specimens, we made use of the PCSOM, which will be further described later in this chapter, a Wild stereo-microscope, and scanning electron microscope (SEM). When using the stereoscopic microscope, if samples consisted of isolated specimens, these were immersed in 100% ethanol following the method of Beynon and Wood (1986). For fragile specimens and teeth attached to mandibulae or maxillae, a soft brush was dipped in ethanol and a few drops of ethanol were then placed on the fractured surface. The specimens were variously rotated to different positions in relation to the light source to acquire the best possible viewing of the striae.

3.2. Enamel Variables Measured in this Study

In the study of ground sections of *H. sapiens*, we recorded the number of striae of Retzius, striae packing pattern, angles of striae of Retzius/EDJ, and cross striation spacing. Both mesial and distal cusps of molars were used. The majority of the fossil material used in this study consists largely of naturally broken tooth surfaces with no control over the plane of fracture. The specimens selected for study showed potential for

observing the features detailed above. In some cases, specimens illustrate one or a few of these features, but in every case we attempted to obtain the most information possible in each specimen for each feature.

Table 3.1. Histological features observed in enamel and their applications in this study, adapted from Ramirez Rozzi (2002).

Histological feature	***Observation***	***Indication***
Striae of Retzius	number	Lateral crown formation time
Striae of Retzius	Tangent to the EDJ	enamel extension rate
Striae of Retzius	length	number of active ameloblasts
Cross striations	Length between adjacent c/s	ameloblast secretory activity
Cross striations	number of c/s between striae	striae periodicity/crown formation time
Prism rods	length x 1.15/ mean daily rates	cuspal enamel development

Conventionally, striae/EDJ angles were measured along three different areas of the EDJ: cuspal, lateral and cervical (Beynon *et al*.; 1991; Beynon & Dean 1995; Rozzi 1993, 2002, Smith *et al*.; 2004) (Figure 3.1A). However, in an attempt to try to identify smaller scale changes in the striae/EDJ angles, we divided the EDJ into five different areas, numbered 1-5 from cusp to cervix (Figure 3.1B). This could not be possible in most cases in the fossil material as striae were very difficult to observe along the EDJ, and thus, striae/EDJ angles was measured as in Figure 3.1A.

The most recent studies in quantifying the angles striae/EDJ in naturally fractured fossil hominids are those of Ramirez Rozzi (1993, 1998, 2002). During the early stages of the development of this thesis work, the author met with Ramirez Rozzi a number of times where the author was shown first hand by Rozzi how to carry out the measuring technique. This training was conducted using sections of modern human teeth as well as sections of great apes. The methodology employed at this stage was similar to that

described in Beynon and Wood (1986) where striae were drawn from photographs onto tracing paper and then the angles were measured using a protractor. After a number of sections, the author and Rozzi independently measured angles in two sections. The results were then compared and the error margin was within 5% of variation. This type of comparison was repeated later in the development of the thesis work using images taken by the author using stereoscopic microscope of fossil teeth immersed in ethanol and ImageJ software. This same software version was used by Rozzi and the author. Again the author and Rozzi independently measured angles on one specimen and the error margin was within 5% difference. The author finally compared measurements taken of the same specimens using both a protractor (as described above) and Image J and almost no differences were found.

Based on these tests, both the author and Rozzi were satisfied with the use of the technique.

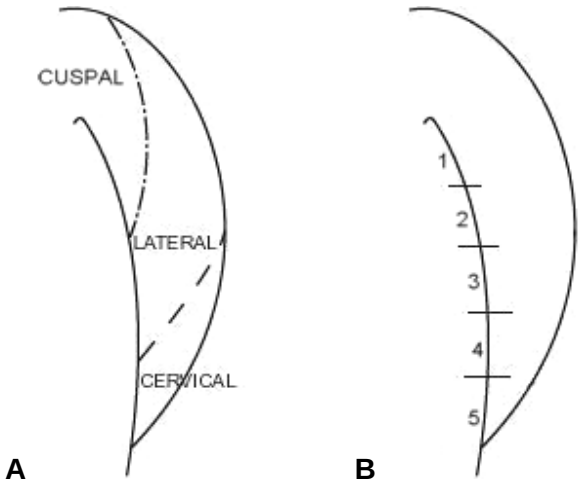

Figures 3.1A and 3.1B. Divisions of the EDJ where striae/EDJ angles were measured in fossils (left) and modern taxa (right).

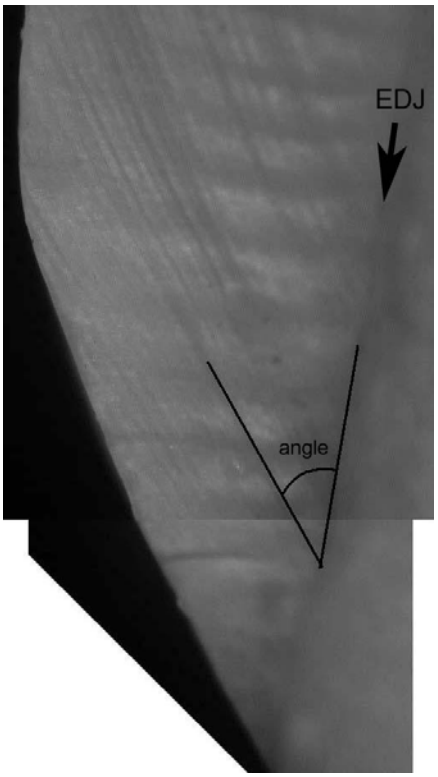

Figure 3.2. An example of the scheme used in this study to measure striae/EDJ angles.

Striae packing patterns on the fossil and extant sample were measured as follows: cuspal height was measured and divided in ten equal divisions, in a similar manner to that described by Dean and Reid (2001a) and Ramirez Rozzi and Bermudez de Castro (2004), and striae were counted in each of these divisions.

Appositional rates or cross striation spacing in both fossil and extant material were measured in a similar manner to that presented by Beynon *et al*.; (1991) in which the enamel crown was divided into cuspal, lateral and cervical enamel (Figure 3.3). Each section was divided into inner, middle and outer enamel. Cross striations were identified as lines coursing perpendicular to the main prism path. In general, at least 3 to 5 adjacent cross striations were measured in as many places as possible in each of the areas indicated in Figure 3.3. This value was then divided by the number of cross striations, which yields a single average value for cross striation spacing in each region.

In the fossil taxa, cross striations occasionally appeared as varicosities (see part 2 of this Chapter). This depended on the diagenesis of the specimen and whether a clearing medium was applied on the surface of the specimen.

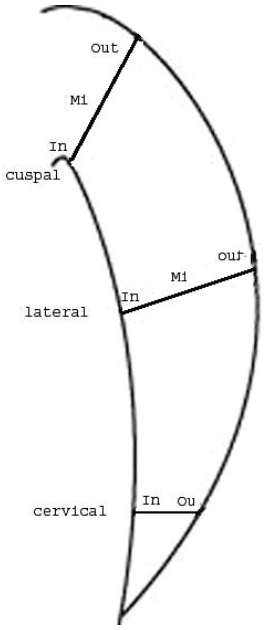

Figure 3.3. Sketch of a cross section of the enamel crown used in our study showing the divisions where cross striations were measured.

Extant teeth used to assess daily appositional rates were prepared by us for this study. Each tooth was carefully removed from its jaw and prepared following protocols described in Reid *et al.*; (1998b). Specimens were embedded in polyester resin and sectioned bucco-lingually along the apices of the mesial or distal cusps, and in one case along the buccal cusps oriented in the mesio-distal plane. Sections of about 150 microns were obtained using an annular saw, which were then lapped down from both sides to a thickness of about 100 microns, aiming to obtain a final section that passed as close as possible to the dentine horns. The sections were subsequently placed in an ultrasonic bath to remove debris, dehydrated and mounted.

3.3. Statistical tests

SPSS (version 14) was employed to run all statistical tests described below, and to graphically represent data. In most cases, due to the low number of specimens available for study in the fossil category, the non-parametric Mann-Whitney *U* test was used to assess differences or similarities of the means of the taxa compared, for example, to assess significance in the values of striae/EDJ between fossil taxa. The Mann-Whitney *U* test compares the means of two sets of groups. To compare values of for example striae/EDJ angles measured in different sections of the same specimen, we used the non-parametric Wilcoxon Signed-Rank test. Statistical significance was established at the p=0.05 level. Descriptive statistics are provided for daily secretion rates of each fossil and extant specimens analysed.

3.4. The portable confocal microscope 1K2S BIO

The development of the portable confocal unit 1K2S BIO was specifically designed as a tool to be used in palaeoanthropological studies but primarily dedicated to the study of hominid hard tissue microstructure (Bromage *et al.;* 2003). The unconventional but highly successful design of the unit 1K2S BIO was carried out by Timothy G. Bromage (New York University, Dental School), Alejandro Perez-Ochoa (University of Madrid) and Alan Boyde (Queen Mary University of London) over a period of three years (2001-2004) (Figure 3.1). A full description of the different stages of its development can be found in Perez-Ochoa (2004). The descriptions that follow in this chapter are based on Bromage *et al*.; (2003, 2005) and Perez-Ochoa (2004).

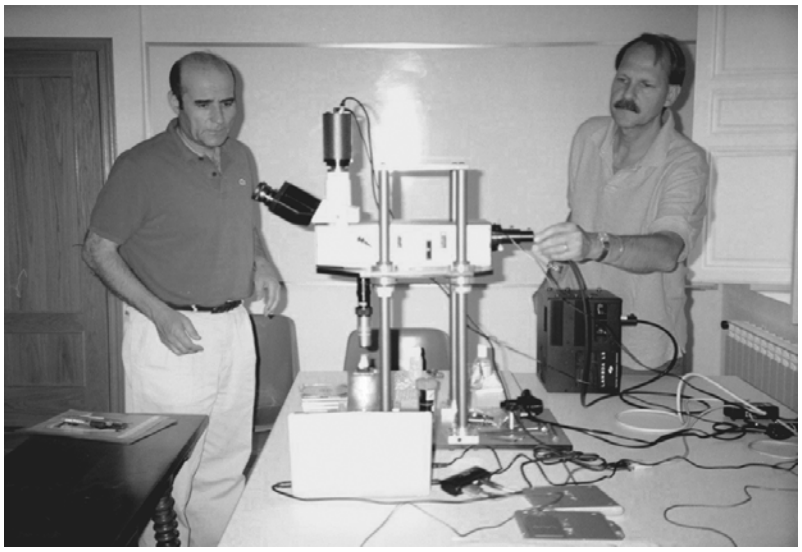

Figure 3.4. Two of the designers of the PCSOM setting up the microscope. T.G. Bromage is on the right side and A. Perez-Ochoa on the left looking at the computer screen. A. Boyde took the picture.

One of the most relevant aspects of this instrument is its portability. This enables its transfer to museums and institutions alike which house the fossil material, avoiding the problem of having to transport these fragile and precious specimens to laboratories outside these institutions, even if appropriate technologies were available nearby, but this was most often not the case. In addition, the use of K2S BIO has the advantage of being completely non-destructive and non-intrusive only requiring that specimen surfaces be clean. Initial applications of the K2S BIO focused mainly on bone tissue, describing and portraying bone collagen fibre orientation in fossil long bones (Bromage *et al.*; 2003). More recently, Perez-Ochoa (2004) and Bromage *et al.*; (2005) indicated the possibility of using the K2S BIO to image microstructural features on dental enamel. The portability of the K2S BIO has been achieved by assembling a number of components which are detailed in the following sections. It must be added that the K2S BIO unit is complemented with an important set of imaging tools and software packages that considerably facilitate the study of enamel features.

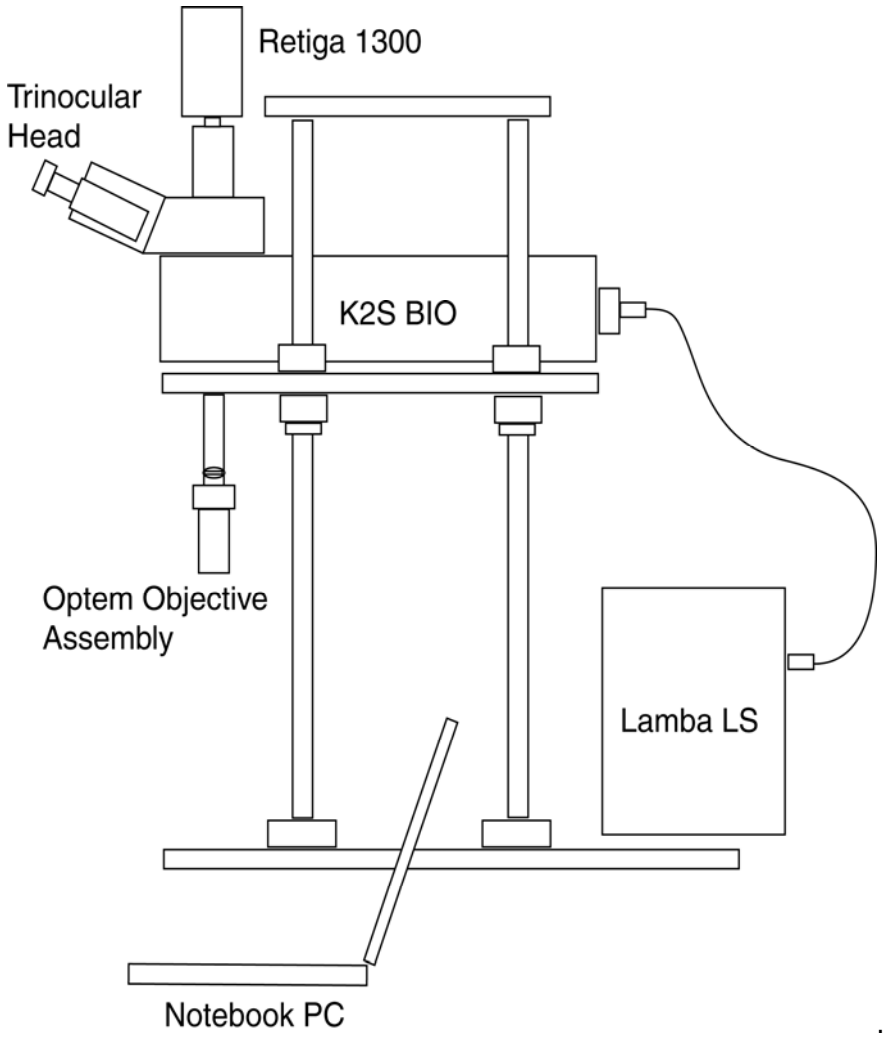

Figure 3.5. Diagrammatic representation of the larger components of the 1K2S BIO (after Bromage *et al*.; 2003). See text for details.

3.5. General features of the confocal unit 1K2S BIO:

Light enters the unit from the rear (Figure 3.6, Number 1). A slider controls the intensity of light (Fig 3.8, Number 2). Light then passes through a diaphragm (Fig 3.8, Number 3) to a filter carrier (Fig 3.8, Number 4). These filters are selected using a slider which has four positions: 1) BF (bright field) 2) RHOD (Rhodamine) 3) FITC (fluorescein) 4) UV (ultraviolet). BF is the selection used when performing reflected light confocal microscopy, while fluorescence microscopy uses the remaining filters. We did not undertake fluorescence imaging for this study.

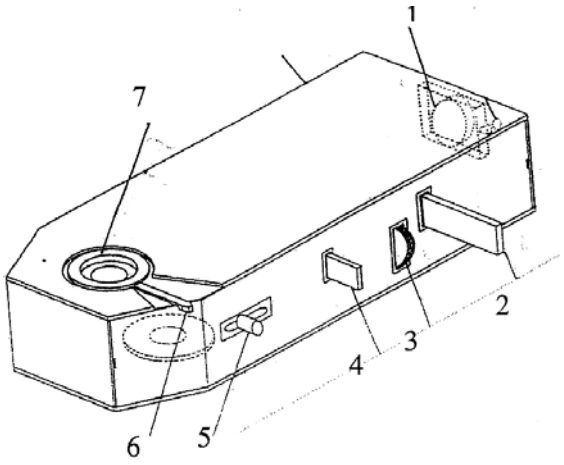

Figure 3.6. Major external features of the confocal unit of the K2. 1) Adapter for light source 2) Slider 3) Aperture 4) Filters 5) Lever used to select the position of Nipkow disc (Confocal 1 – CF1- Confocal 2 –CF 2- and bright field –BF-). 6) Lever to select direct viewing or CCD 7) Fitting for trinocular head.

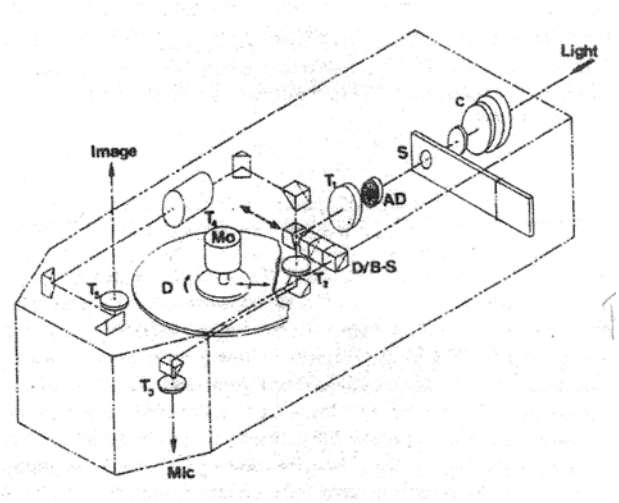

Figure 3.7. Internal configuration of the Technical Instrument Co. K2S-BIO confocal scanning optical microscope module. Light enters from the rear, passes through optical elements to a beam splitter, which is then transmitted through the Nipkow disk and to the microscope optics and the specimen. Light reflected from the specimen passes back up through the microscope optics and Nipkow disk to the beam splitter, which now conveys the light to the Image plane of the eyepieces or camera.

This portable unit contains a Nipkow disc which can be switched between slits and pinhole apertures while in motion (Figure 3.8). The disc is penetrated by numerous (thousands) of interlaced pinholes that, when illuminated from one side, scans light

across the specimen and, because of the geometry of returned reflected light from the specimen, allows only that light emanating from the plane of focus of the objective lens to return through the pinholes and to the eyepieces or camera. Selection of slits or pinholes is controlled by a slider (Fig 3.6, Number 5). The disc is plated with a thin layer of black chrome on one side and is tilted at 5.25 degrees to eliminate unwanted light reflected back from the disc. The tilt causes reflected light from solid portions of the disc to be re-directed to a light trap. This system also uses cross polarizing filters and a quarter wave plate to stop any unwanted reflected light. An important advantage of using one side of the disc for both illumination and observation is that the alignment of the optics is not so critical.

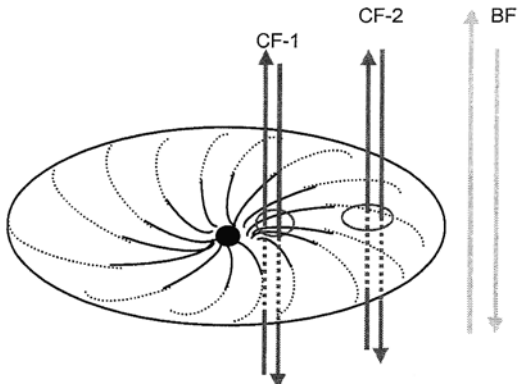

Figure 3.8. Nipkow disc fitted inside the confocal unit. Confocal 1 (CF1) which uses pin-holes, confocal 2 (CF2) uses slits and bright field (BF) does not use the disc.

3.6. Illumination system

A Lambda LS Xenon Arc Lamp is fitted with a pre-aligned mirror contained within a brass heat sink. The lamp has 175 watts having 320nm to 700nm output in an ozone-free bulb. Voltage can be set to 110V or 220V. Even illumination is achieved with a liquid light guide whose input end sleeve fits into the Lambda LS tube. The illuminating beam is focused by the parabolic mirror and lens tube onto the end of the light guide. The

position of the output end-sleeve, which is coupled onto the external K2's Nikon lamp housing adapter tube, can be adjusted to produce an optimised collimated light beam.

3.7. Optical configuration

The confocal unit is equipped with a trinocular head having a Nikon style bayonet mount to which is attached a Seidentopf binocular fitted with 10x eyepiece objectives angled at 30^{o} to the optical axis. This head allows 100% of the light to be viewed in the Nikon style oculars or diverted to 14% visual and 86% to photo/video.

The objective lenses thread into a coaxial manual coarse/fine focus module whose flange inserts into a bayonet coupler secured by a thumb screw to the Nikon style objective turret mount below the K2 (Figure 3.5). A custom modification included a finite to infinity tube length converting lens. Infinity corrected objectives for the K2 include Optem 10x (0.45 NA, 19 mm WD) and Mitutoyo 20x (0.42 NA, 20 mm WD) lenses. The K2 uses a 4-pin IEEE 1394 high resolution 12 bit monochrome QIMAGING Retiga 1300 camera (Burnaby, BC, Canada). Flexibility in magnification was met with CCD mount adapters of varying magnification (0.5x; 1.0x and 1.9x)

3.8. Image Acquisition

The 1K2S BIO returns image detail from the surface plane or from immediately below the surface to a high resolution 12 bit monochrome QIMAGING Retiga 1300 camera mounted on the trinocular head. The camera contains a 2/3" monochrome progressive scan interline CCD containing 1280 x 1024 pixels of 6.7 µm x 6.7 µm in size. Real time previewing capability facilitates camera set up conditions, which are adjusted by software interface. Adjustments include integration time, gain and offset. An electronic shutter prevents additional unwanted vibrations.

To obtain two-or three dimensional projections from rough surfaces, the potential fields must be compiled from a series of images captured at different optical planes represented in the z-axis of the field of view and which are collected manually.

3.9. Software and Hardware

To reconstruct all optical planes in two or three dimensions across the field of view, Syncroscopy AutoMontage software (Frederick, Maryland) was used. This software was designed to compile focused image content from a series of images at different image planes. There is no practical limit to the number of images that may be acquired in succession. Images are automatically numbered for saving at the end of an imaging routine. An additional benefit in confocal applications is that any overlapping image content is recognized and represented only once on the basis of peak grey level. Thus two dimensional projections derived form a through series appear as though they had been derived from one image plane.

A Sony VAIO notebook PC computer (VAIO SR 33- 650 MHz, 256 RAM) was used to capture images. Plug-play software interface to the QIMAGING QCapture imaging program was used.

AutoMontage was used in measurements of features collected using the PCSOM, which included enamel thickness, cross striation spacing, distance between striae of Retzius and generally perikymata counts in fossil specimens.

3.10. K2 scales

To calibrate the lenses and adapters, a stage micrometer was used with each lens and adapter combination. Images were obtained of the micrometer and from each image; and the software was thus calibrated on the basis of measurements taken between two points of known distance. This information was then saved and labelled in software for each combination. The width of field for each adapter was:

Table 3.2.

LENS	1:1 adapter		
	FW (µm)	microns/pix	pix/microns
5x	1900	1.4855	0.6731
10x	950	0.7427	1.3463
20x	475	0.3713	2.6926
50x	190	0.1485	6.315

Table 3.3.

LENS	0.5 adapter		
	FW (µm)	microns/pix	pix/microns
5x	3650	2.8537	0.3504
10x	1825	1.4268	0.7008
20x	912.5	0.7134	1.4016
50x	365	0.2853	3.5041

Once images are opened in AutoMonatge and the calibration is selected, the software allows for direct measurements to be made between two points. This method was used in measurements of cross striation spacing observed with the PCSOM only in the fossil material.

3.11. Use of media and cover slip

The question concerning coverslip media is interesting, one that we also asked ourselves at first and then resolved to our satisfaction. Some technical issues of this technique are addressed first, followed by some more detailed information of the use of media in published records.

The design of the microscope was guided by the nature of the sort of samples encountered in our work, in which because of potentially large variations in specimen topography, very long working distance lenses were employed (e.g. 20 mm). For such a microscope, the only practical illuminating beam is one in which the focusing lenses at

both the lamp housing and input ends are adjusted to provide a light beam that is parallel with the optical axis and normal to the imaging plane. Specularly reflecting subsurface specimen details return light normal to that surface, and thus the refractive index of the coverslip medium makes no contribution to an optical path difference. The vast majority of the light reflecting from subsurface details is specular, and it is this light that forms the image. There is internally scattered light from the focused on plane that is on-specular, however most of this light is lost to the imaging system. Take a subsurface object reflecting light obliquely to the surface. A ray passing through the specimen into, say, 20 micrometres of ethanol (RI = 1.36) will diverge away from normal ever so slightly from that of immersion oil (RI = 1.52). Upon encountering the coverslip, the ray in ethanol bends back toward normal, converging on the ray in oil, crossing it, and emerging on the side of optical center. Both ethanol and oil rays emerge from the coverslip, bending away from normal, subparallel and largely lost because of their obliquity to a very long working distance lens of low numerical aperture. Less obliquely scattered rays from subsurface details will have such a small deviation owing to the opical path difference between ethanol and oil as to be less than the wavelength of visible light and thus irrelevant. If there were any measurement concerns, they would be in the Z direction and at significant depth. However, as we collapse all Z planes over only ca. 1-20 micrometres (1-50 rarely) into one 2D image for purposes of measurements in X and Y, this difference also is irrelevant. The Portable Confocal Scanning Optical Microscope is a superb specular reflection microscope, which, while posing severe limitations on the light gathered, provides research grade and non-destructive imaging of histological details heretofore unavailable in early hominin research.

The use of immersion oil is completely harmless to the specimen and it is commonly used in studies of laser confocal microscopy in molecular and cellular biology

as well as in other aspects of confocal work where objects need to be studied at high magnification. The application of immersion oil to the sample does not change the features studied in any way, it only increases the birefringence of the area studied, and bringing more contrast to the features under study. No direct measurements were undertaken between a dry sample and a sample studied under the microscope using immersion oil except in one specimen Stw 402 for which striae of Retzius were counted in the same area before and after the application of immersion oil, which were the same. Ethanol is harmless for the specimen. It was originally used by Beynon & Wood (1986). Similarly to immersion oil, ethanol only increases the birefringence of a given feature by generating contrast with the surrounding areas. In Beynon & Wood (1986; pp: 184- 186) it is noted that "*immersion of the specimen in ethanol…improves optical contrast by reducing reflective highlights and enhances visualization of striae of Retzius. The mechanisms of this latter effect may be linked with their hypomineralization and increased microporosity*". The studies of Beynon & Wood (1986, 1987) and those of Beynon & Dean (1988), Ramirez Rozzi (1993, 1998) all used the same methodology of either applying a drop of ethanol in the area studied or completely immersed the specimen in the medium. In Figure 1 of the JHE publication, as explained above, measurements were carried out between a specimen immersed in ethanol and the same specimen with immersion oil. The measurements of the distance between striae were the same.

SECTION 2: Materials

3.12. Modern taxa

Reid *et al*.; (1998a) sectioned teeth of four individuals from a Medieval French population discovered at the archaeological site of La Picardie, which were made available for this study (Tables 3.5 and Table 3.6). The methodology of counting striae employed by Reid *et al*.; (1998a) consisted of measuring the height of the mesial and buccal molar cusps in millimetres from the cervix to the cusp tips. However, the present study employs a different methodology, already described earlier in this chapter in which the cusps were measured and divided in ten equal divisions following protocols detailed in Dean and Reid (2001). Therefore results from both studies are only comparable at the level of total counts of the striae of Retzius, and not to the individual values obtained for each of the sections measured. Because of the methodological difference, some teeth included in Read *et al.*; (1998a) could not be sampled in this study because in heavily worn teeth the cusp outline could not be reconstructed.

Some sections, however, not used by us for accessing the total numbers of striae, were used for estimations of angle variation between the striae and the EDJ. This measure is not affected by attrition of the cusps since the measurements are taken by divisions of the EDJ. Therefore, if the dentinal area had suffered minimal attrition but could be easily reconstructed, these sections were used for angle measurements.

To assess daily appositional rates in *H. sapiens*, ten molar sections were prepared for this study (Table 3.7). These specimens derive from an archaeological site in France known as the Merovingios, as well as some derived from a dental practice in Paris.

Table 3.4. Specimens sectioned by Reid *et al.*; (1998a) used to measure angles striae/EDJ. [lo=lower; up= upper; L= left; R= right; M1, M2, M3= first, second and third molar; Mes= mesial; Dis= distal; LF= lingual face; BF= buccal face]

Specimen	Tooth type and face	Specimen	Tooth type and face
T 49	UP L M3 MES LF	**EN 13**	LO R M1 MES 2 PRO
	UP L M3 MES BF-1		LO R M1 MES 2 MET
	UP L M3 MES BF-2		LO R M1 MES PROT
	UP R M3 MES BF		LO L M2 MES META
	LO L M3 MES BF		UP L M2 MES PAR
	LO L M3 MES LF		LO L M1?
	LO L M3 DIS BF		LO L M1 DIST ENTOC
	UP L M2 DIS BF		LO L M1 MES PROT
	UP L M2 DIS LF		LO L M2 MES PROT
	LO L M2 MES BF		LO ?
	LO L M2 MES LF		
	LO L M2 DIS BF		

Table 3.5. Specimens sectioned by Reid *et al.*; (1998a) used to study striae packing patterns. [lo=lower; up= upper; M1, M2, M3= first, second and third molar; Mes= mesial; Dis= distal; LF= lingual face; BF= buccal face].

Specimen	Tooth type and face	Specimen	Tooth type and face
EN 13	LO L M1 MES BF	**T 49**	LO L M1 MES BF
	LO L M1 DIST BF		UP L M2 MES BF
	LO L M1 DIST LF		LO L M2 MES BF
	LO L M2 MES BF		UP R M3 MES BF
	LO L M2 MES LF		LO L M3 MES BF
	LO L M2 DIST LF		LO L M3 MES LF
			LO L M3 DIS LF
			UP L M3 MES 1 LF
			UP L M3 MES 1 BF
			UP L M3 MES 2 BF

Table 3.6. Specimens from the Merovingio's collection as well as modern human samples derived from a dental office in Paris that were used to obtain cross striation spacing. [lo=lower; up= upper; M1, M2, M3= first, second and third molar; Mes= mesial; Dis= distal; LF= lingual face; BF= buccal face]

Spec.	Tooth type and face
SEP	lo M2 Mes-BF
SEP	lo M2 Dis-LF
F 54	up M1 Mes-BF
F 54	upp M2 Mes-BF
F 83	lo M1 Mes-LF
F 83	lo M1 Dis-LF
F 83	lo M1 DF* mes-dis cut
MH 1	up M1 Mes-BF
MH 2	lo M3 Dis- LF
MH 3	lo M1 Mes-LF

3.13. Fossil samples

Molars surveyed for this study are shown in Table 3.8. After a preliminary analysis using stereoscopic microscope and the PCSOM, a subset of these specimens were selected for further analysis (Table 3.9). It should be noted that we have used the catalogue numbers as per the records kept at the fossil repositories throughout this study, however, two specimens from Sterkfontein -STW 284 and Stw 217- are referred to by Moggi-Cecchi *et al*.; (in press) as STW 280 and Stw 208 respectively.

Table 3.7. Fossil specimens surveyed in this study

Transvaal Museum
Swartkrans: - SK: 12, 19, 37, 35, 37, 47, 52, 833, 844, 849, 864, 855, 870, 1524, 1594, 4769. - SKX: 268, 864, 866, 21841, 3356, 5024, 6277, 19892. - SKW: 5, 10, 11, 55, 4768, 4769, 3068. Kromdraai: KB 5223, TM PAL 99. Sterkfontein: - STS: 17, 18, 19, 52, 61, 72, 1579.
Dept. of Anatomy:
Sterkfontein: - STW: 12, 14, 73, 18, 34, 37, 71, 90, 96, 142, 212, 215, 276, 284, 285, 313, 325, 402, 529, 542, 574. Makapansgat: - MLD: 4, 11, 12, 18, 28, 41.
Gondolin: GAD 1, and 2

Table 3.8. Specimens of fossil taxa included in this study.

A. africanus			***P. robustus***		
Specimen	**Tooth Type**	**Cusp**	**Specimen**	**Tooth Type**	**Cusp**
Stw 402	M^1	protocone	SK 849	M^1	paracone
Stw 252 K	M^1	mes-grooves	SKW 11	M^2	metacone
Stw 217	M^1	metacone	SKW 4768	M^2	hypocone
Stw 284	M^2	protocone	SK 35	M_2	metaconid
Stw 71	M^2	protocone	SK 37	M_2	hypoconid
Stw 37	M^3	hypocone	SK 55	M_2	hypoconid
Stw 252 H	M^3	mes cusps	SKW 4769	M_2	protoconid
Stw 11	M^3	metacone	SKX 21841	M^3	paracone

Stw 285	M_2	entoconid	SK 875	frg	
Stw 96	M_3	metaconid	SKW 4771	frg	
Stw 90	M_3	protoconid	TM 99	frg	
Stw 93	?	?	KB 5223?	**M_1**	Prod/metd
Stw 190	frg	hypocone			
Stw 325	?	?			
Stw 590	frg	?			

3.14. Descriptions of fossil specimens

Images of the fossil specimens studied can be found in Appendix 1. The specimen descriptions given below are not aimed to provide detailed morphological descriptions, as these can be found in Robinson (1956); Grine (1982, 1993); Grine and Martin (1988), and Moggi-Cecchi *et al*.; (in press), but only to serve as a reference of the areas studied in each specimen.

3.14.1. Sterkfontein:

Stw 11: This specimen is an incomplete isolated RM^3 with only a very small portion of the root preserved (about 3.7 mm) on the metacone. Only the buccal cusps are preserved and wear is moderate, but there is about 0.7 mm of enamel over the dentine. Metacone crown height (CH) is about 4.9 mm.

Stw 37: This specimen is an isolated LM^3 missing most of both distal cusps. The crown outline is asymmetric and pitting can be observed in the enamel. No roots are preserved and wear is moderate. A groove-like Carabelli is present. Metacone CH is 7.5 mm.

Stw 40: This specimen is a maxillary fragment encased in matrix which also preserves an incomplete RM^2. Part of the root of the paracone is preserved. The main preserved cusps, the paracone and metacone, are worn.

Stw 71: This specimen is an isolated RM^2 that only preserves the distal half of the worn crown. The root is about 14.2 mm in the metacone. Cusps are worn nearly flat, although the presence of a distoconule can be identified. Metacone CH is 5.95 mm.

Stw 90: This is an isolated developing crown of an RM_3 lacking roots. All main cusps are present although there is some enamel missing in the protoconid. There is a well developed C6. The specimen is covered in places by a manganese layer. Protoconid CH is 8.3 mm.

Stw 93: Molar fragment.

Stw 96: This specimen is an incomplete crown of a LM3 missing the enamel anterior to both mesial cusps. The base is wide and there is about 7 mm of root preserved in the entoconid. A C7 can be identified. Metaconid CH is 6.3 mm.

Stw 188: This specimen is an isolated and complete crown of a RM2 lacking roots. The specimen is cracked bucco-lingually dividing the mesial and distal moieties in almost equally large halves. Wear is slight and the base of the crown appears broad. Two small cuspules can be identified in the distal margin and there is a hypoplastic groove on the buccal area. Carabelli is present as a pit. Metaconid CH is 7.8 mm.

Stw 208/217: This specimen consists of the buccal half of a RM^1 and part of the hypocone preserving about 10.6 mm of roots which were still forming. Wear is moderate. Hypocone CH is 8.1 mm.

Stw 252 H: This specimen is a complete crown of a RM^3 preserving only about 3.4 mm of the roots. A mesio-distal crack splits the crown in halves being the lingual half larger. Carabellis is well expressed and protocone is divided by a groove. The base of the tooth is broad. CH of the studied area, between the mesial cusps, was estimated to be approximately 7 mm.

Stw 252 K: This specimen consists of the distal half of the RM^1crown with moderate wear and preserving about 3.4 mm of the metacone root.

Stw 284/280: This specimen consists of a complete crown of an LM^2 almost unworn. This specimen had been sectioned along the apex of the mesial cusps by Grine and Martin (1988). The tips of the main cusps are close together giving the tooth crown a broad base appearance. Carabelli is present as a pit. All roots, although broken, are present. CH of the protocone is 10.9 mm.

Stw 285: This specimen consists of the antemeres of L and RM_2. The specimen studied here is the RM_2 which lacks most of the mesial and buccal portion of the protoconid and the mesial aspect of the metaconid. No C6 or C7 are present. Wear is moderate. The disto-lingual quadrant preserves about 10 mm of the root. CH of the metaconid is 7.2 mm.

Stw 402: This specimen consists of an unworn complete crown of RM1. Similarly to Stw 284/280 cusps tips are positioned close together giving this tooth a broad base appearance. This specimen had been previously sectioned by Grine and Martin (1988) along the tips of the distal cusps. Carabelli is well developed, and a distoconule can be identified between the hypocone and metacone. Roots appear to have been forming at the time of death, with about 8.2 mm preserved in the protocone. Metacone CH is 9.2 mm.

3.14.2. Swartkrans:

SK 35: This incomplete specimen consists of the protoconid and a mesial fragment of the hypoconid of a RM_2. Wear is slight. The plane of fracture passes perpendicular to the mesio-marginal ridge. CH 6.2 mm

SK 37: This specimen consists of a left mandibular fragment with an incomplete M_2 and complete M_3. The specimen studied was the M_2 which preserves the part of the hypoconid and a distal fragment of the hypoconulid. Wear is moderate. Hypoconid CH is 7.8 mm.

SK 55: Mandibular fragment preserving right P_4 to M_3 and left P_3 to M_2, which was the specimen studied. This tooth is missing the distal moiety. Mesial cusps are complete and wear is moderate. In this specimen, cuspal striae of Retzius could be easily observed when the specimen was immersed in ethanol. Hypoconid CH 9.1 mm.

SK 875: Tooth fragment catalogued as part of a third molar.

SK 849: This specimen is a nearly complete crown of a left M^1 showing only slight wear and missing a wedge of enamel in the paracone. Roots are preserved measuring about 8.5 mm in the metacone. Paracone CH 8.5 mm.

SKW 11: Maxillary fragment with right P^3 to M^3 and left M^2 and M^3. The M^2 is incomplete, preserving the lingual half of the tooth. Wear is slight. Protocone CH is 6.1 m.

SKW 4768: This incomplete LM^2 preserves the metacone and a distal fragment of the hypocone, which was the face studied. The root in the metacone had completely developed and about 14.1 mm are preserved. Wear is moderate. Metacone CH 7 mm.

SKW 4769: This specimen is an incomplete LM2 fractured bucco-lingually mid-way between the mesial and distal moieties and missing a portion of the metaconid. Wear is moderate. There are about 12.2 mm of root preserved. Striae were visible in the proximal and distal halves of the lingual area. CH in proximal is 6.1 mm and 5.8 on the distal half.

SKX 21841: This specimen consists of an unworn RM^3. The crown is complete and about 7 mm of the root is preserved. This tooth was originally sectioned by Grine and Martin (1988) along the apex of the mesial cusps. The occlusal area is complex, with two small cuspules in the mesio-marginal ridge complex. All main cusps are well developed. Carabelli cusp is present as a small furrow.

3. 14.3. Kromdraai:

KB 5223: This specimen consists of isolated lower teeth of a single individual preserving the first permanent molars and incisors as well as part of the deciduous dentition. Both

M_1 are preserved and practically unworn. The RM_1 is of relevance as this was the tooth originally sectioned along the mesial cusps by Grine and Martin (1988). This specimen was first described by Grine (1982). The RM_1 has completed crown but no root is present. The specimen is covered in manganese accretions making difficult to count perikymata, which are otherwise clearly visible in the remaining areas. The RM_1 has a prominent postmetaconulid which Braga and Thackeray (2003) refer to as a C7. No C6 is present.

TM PAL 99: This specimen is a molar fragment.

CHAPTER 3- PART 2

3(2).1. Imaging fossil enamel using PCSOM (Methods part 2).

The main objective of this chapter is to illustrate images of enamel microstructural features obtained during the course of this study using the PCSOM, which show a wide range of capabilities of this instrument. We detail more specifically the methodology used for the acquisition of each image and its relevance to the study of fossil hominid enamel. The images below begin with the external enamel surface at low magnification, followed by details of microstructures preserved inside the enamel cap at higher magnification.

During the course of this study, more than 1000 images were taken of about 40 teeth representing at least three fossil taxa, *A. africanus, P. robustus* and early *Homo.* These specimens are housed at the Department of Anatomy, Medical School, University of the Witwatersrand; or the Transvaal Museum, Pretoria. Some of the images shown here may have been used in the publication section (Chapters 9-11).

For the most part, the techniques used in this study are quite simple and do not vary much between samples. However, there were no previously established protocols for the use of the PCSOM on fossil enamel, so these were established during the conduct of this study. In the majority of cases illustrated below, internal enamel structures were imaged from natural fractures, which meant that we regularly imaged topographically complex surfaces over distances separated by only a few microns.

In general, the average specimen fracture plane was placed at an angle of about 5-7 degrees to the lens. When immersion oil was used between the specimen and a coverslip, angulation of the specimen became more critical, because if perfectly plane to the optical axis, specular light reflected back to the objective lens from the coverslip would make imaging impossible. Further, when a cover slip was used, the glass often

had to be broken to fit the surface studied. Images indicate field width (FW), adapters used and confocal selection (CF 1= pin holes; CF 2= slits).

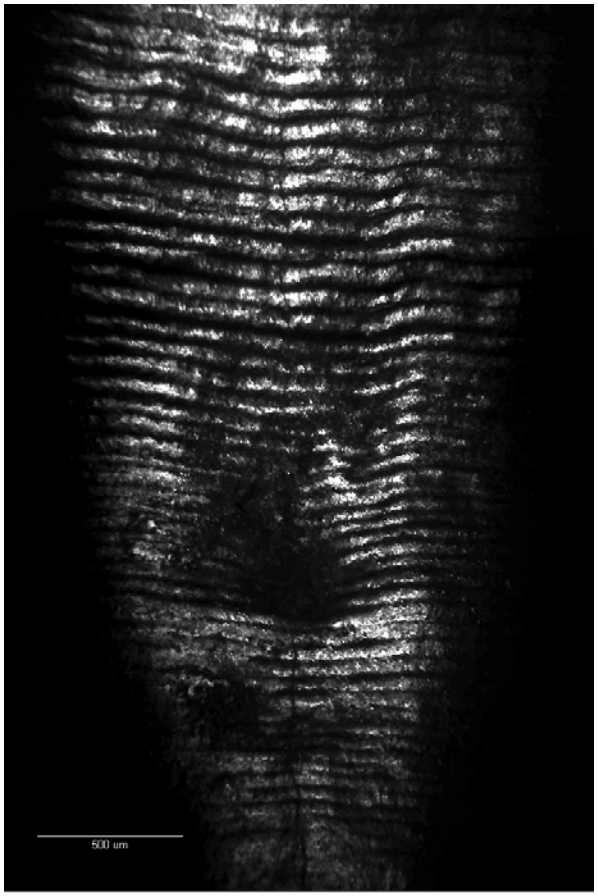

Figure 3(2).1a. Specimen KB 5223, a lower right central incisor from Kromdraai B. Perikymata are the horizontal bands in the 3.6 mm of the crown shown here. This tooth was originally described as *P*. *robustus* (Grine 1982) and later as *Homo* (Braga & Thackeray 2003). Image taken using 5x lens and 0.5 adapter. Scale 500 µm. CF 1.

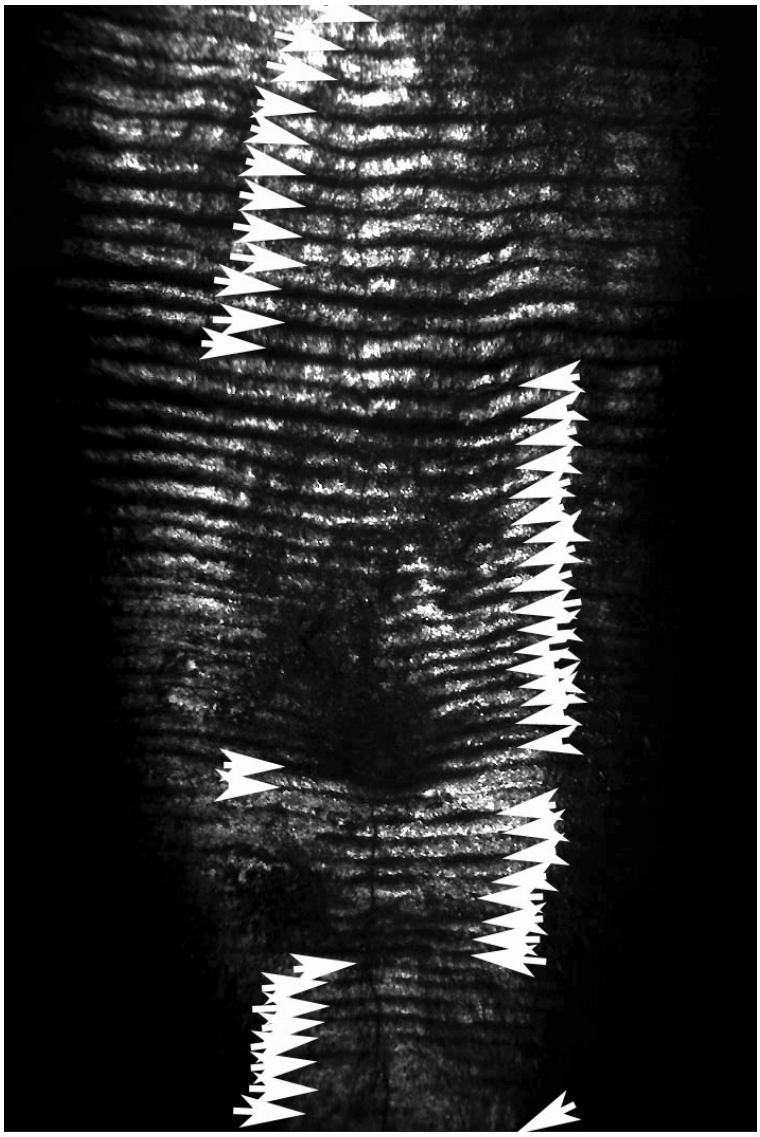

Figure 3(2).1.b. Specimen KB 5223. Arrows mark the location of the 48 perikymata counted in the 3.9 mm of the crown of this specimen. The total crown height of this incisor is 9.6 mm and a total of 86 perikymata were counted on the crown of this tooth. Beynon & Wood (1988) noted that it was a characteristic of P. *robustus* incisors to show a perikymata pattern so evenly spaced near the cervix.

Both images; 3.(2).1a and 3.(2).1b, were manually montaged in Adobe from two different fields independently montaged in Synchroscopy from about 5-6 images each.

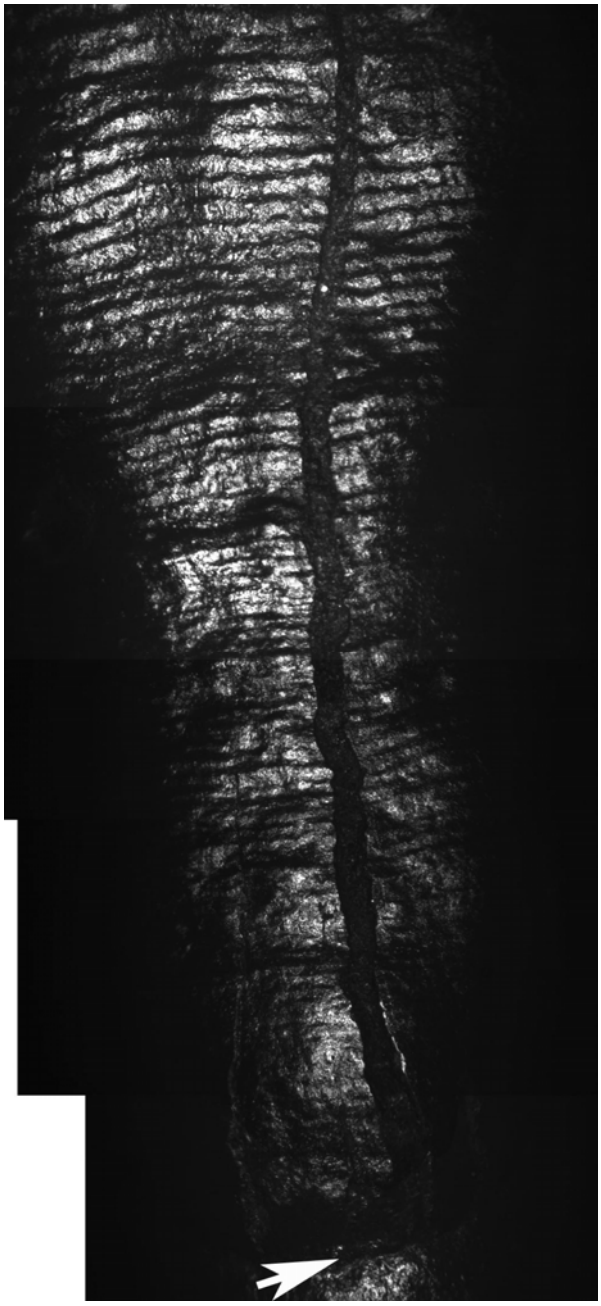

Figure 3(2).2. Specimen Stw 151 from Sterkfontein originally described by Moggi-Cecchi *et al*.; (1998). On this tooth, a RI_1, a total of 103 perikymata were counted by Moggi-Cecchi *et al*.; (1998), which is similar to the number observed for other *A. africanus* specimens. However, other features preserved on the craniofacial bones of Stw 151, show a more *Homo* like morphology (Moggi-Cecchi *et al*.; 1998). This, together with the unclear stratigraphic position of the specimen, Members 4 or 5 of Sterkfontein, made its taxonomic attribution inconclusive. White arrow marks the cemento-enamel junction. The crown shown here (about 6 mm) contains approximately 78 perikymata. This image was compiled from three different fields montaged in Synchroscopy. 5x lens and 0.5 adapter were used in imaging this specimen. FW. 2.5 mm. CF 1.

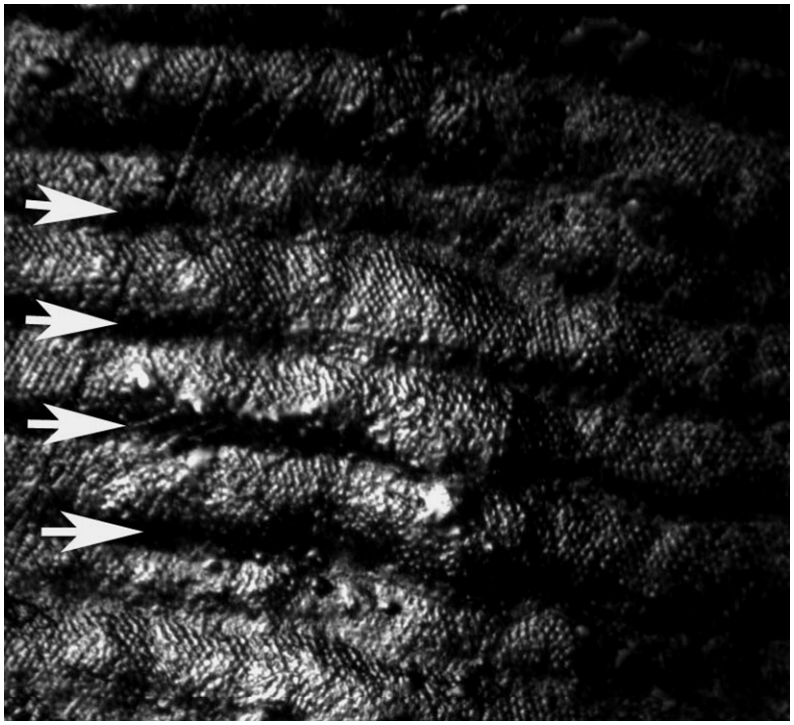

Figure 3(2).3. Surface of the enamel of an *A. africanus* premolar taken near the cervix. Perikymata are shown in white arrows. This image was obtained using 20x and 1:1 adapter. Tomes process pits (prism ends) can be seen as small circles stacked up on each other between perikymata. FW 325 µm. CF 2.

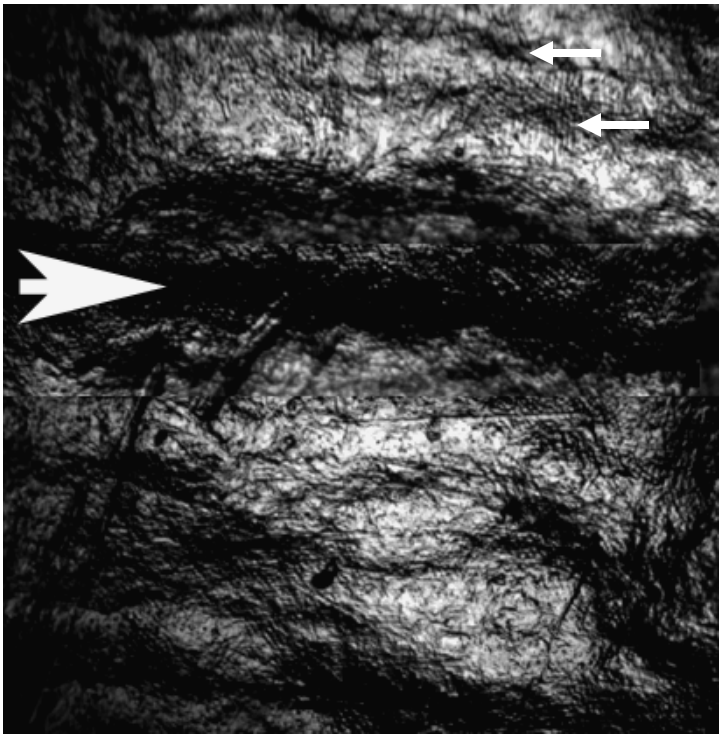

Figure 3(2).4. Image of the lower right first permanent molar of Taung taken near the cervix and showing an abnormal phase of enamel deposition in the form of a deep grove or hypoplasia (large white arrow). Small white arrows indicate normal perikymata. Scratches are also noticeable on the surface of this tooth. This image was taken using 20x lens and 1.8 adapter. Two different fields are represented in this montaged image. FW 263 µm. CF 2.

Figure 3(2).5. Cervix of the left M_1 of Taung showing preparation marks (black arrows) and enamel defects known as broches (white arrows). The dots represent Tomes process pits. 20x lens with 1.8 adapter. FW 135 µm. CF 1.

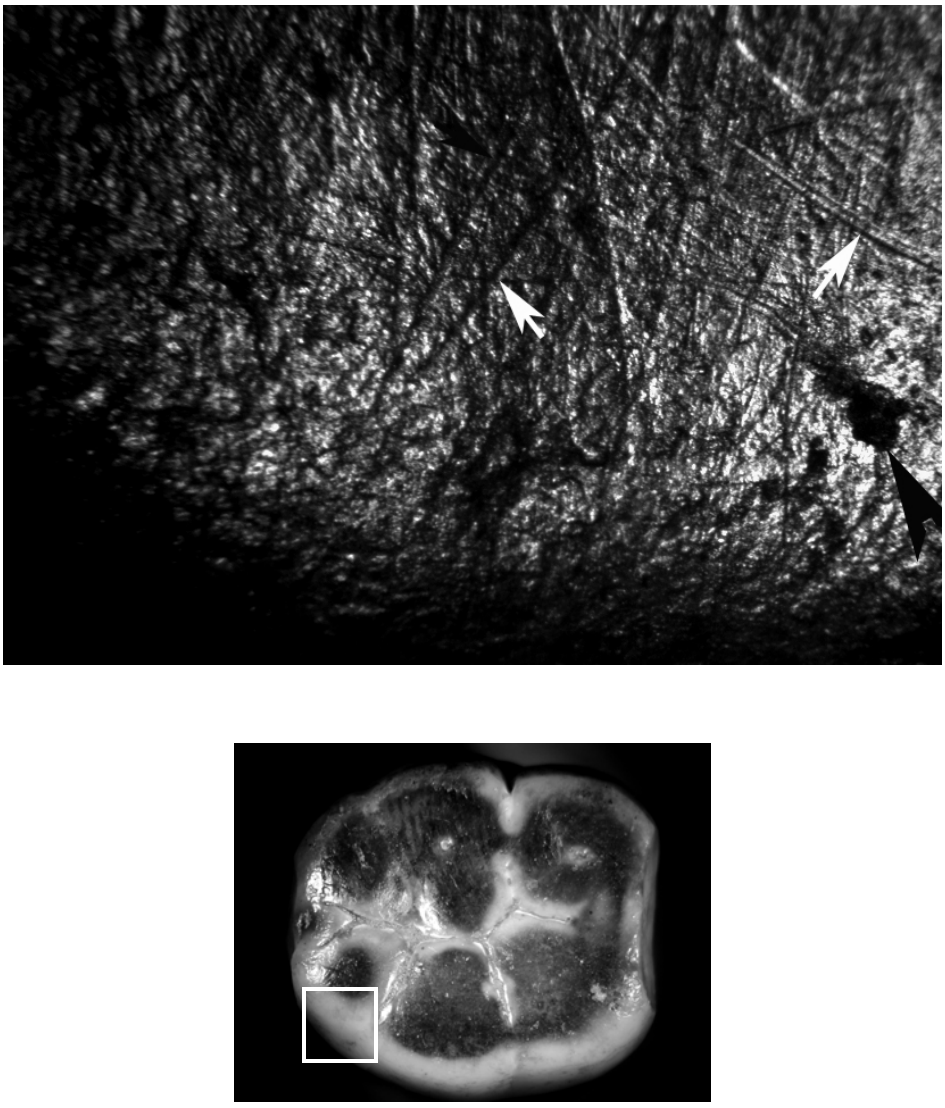

Figure 3(2).6. Image of the crown surface of GD 2, the largest *Paranthropus* molar recorded in South Africa, recovered during ex-situ excavations at the site of Gondolin. The top image shows scratches (white arrows) and pitting (black arrow) derived from food processing during life. 5x lens and 0.5 adapter (FW 2.5 mm, CF 1). The specimen GD 2 measures 18.8 (MD) and 18.1 (BL) (Menter *et al.*; 1999)

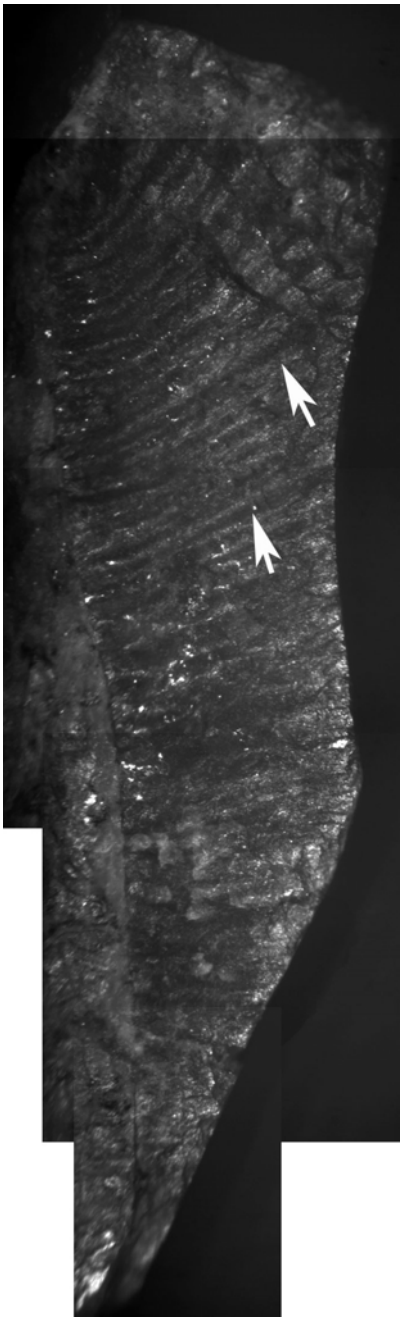

Figure 3(2).7. This fragment of a molar was recovered from the site of Gondolin, South Africa. It's taxonomic attribution has been problematic because of the incomplete nature of the specimen, but it has been suggested that it was possibly not *Paranthropus* (Menter *et al*.; 1999). However, measurements of the striae/edj angles indicate low angle values similar to other *Paranthropus* specimens, and the shape of the HSB are long and thin (white arrows) as in other *Paranthropus* specimens, thus it most likely belongs to this taxon. FW 1.88 mm. CF 1.

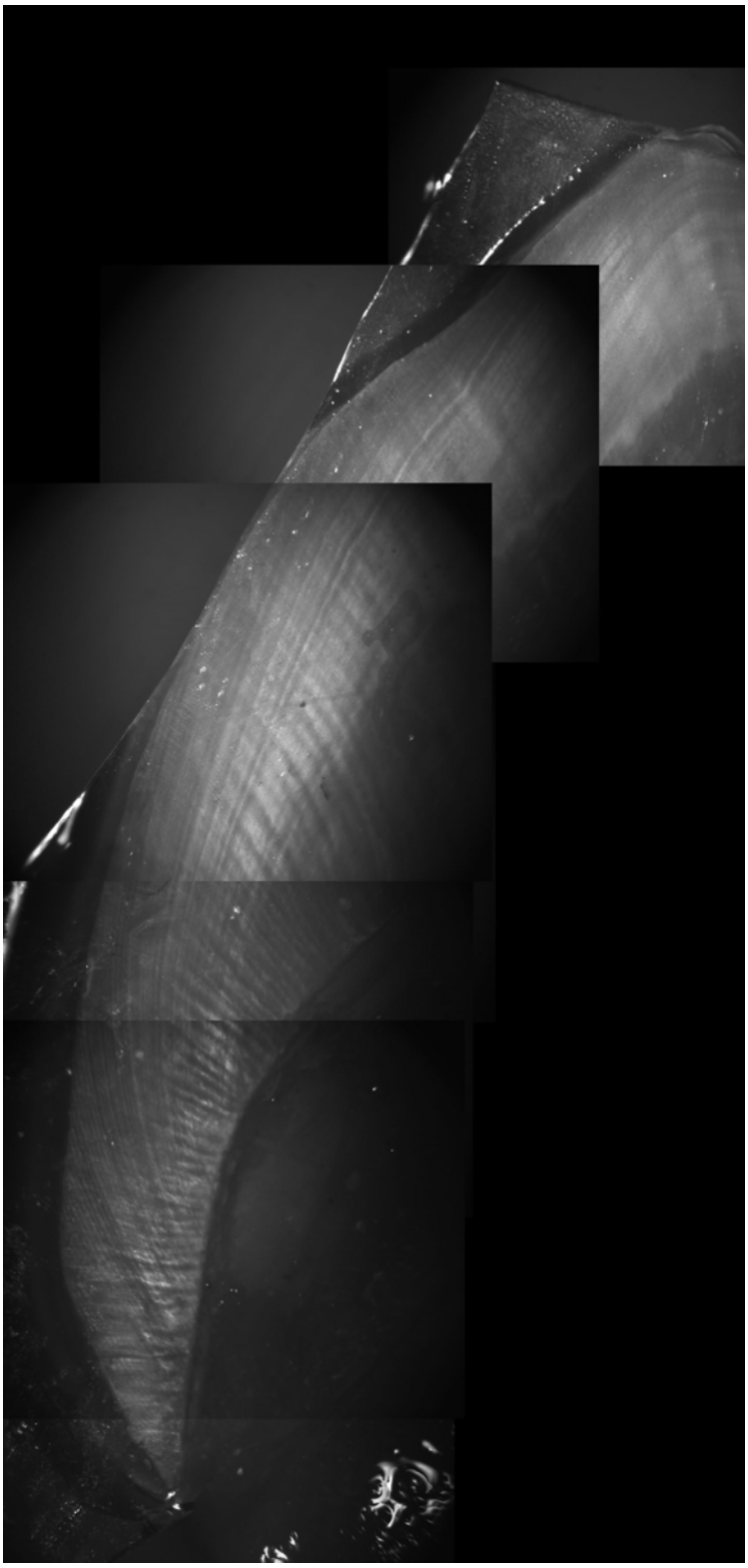

Figure 3(2).8.Montage of the paracone of *P. robustus* specimen SKX 21841 from Swartkrans Member 3. We counted 56 lateral striae on the face shown in this image. We used a 5x lens and 0.5 adapter, clearing medium and a cover slip. CF 1.

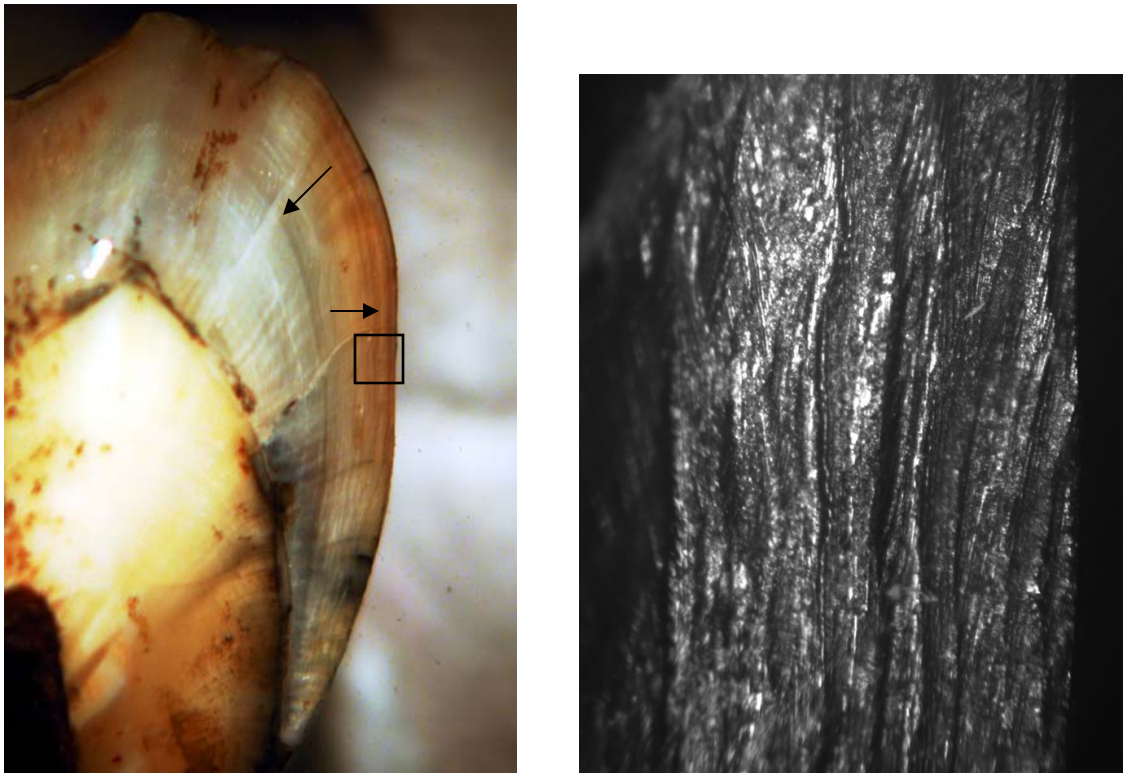

Figure 3(2). 9. Specimen SK 1524 (*P. robustus*). The image at left was taken by immersing the specimen in ethanol and photographed using a stereoscopic microscope. Seemingly marked striae appear on this image. Closer inspection under the PCSOM showed that the apparent striae are scratches (image at right image). 10x lens and 1:1 adapter, no clearing medium was used. FW 0.5 mm. CF 2.

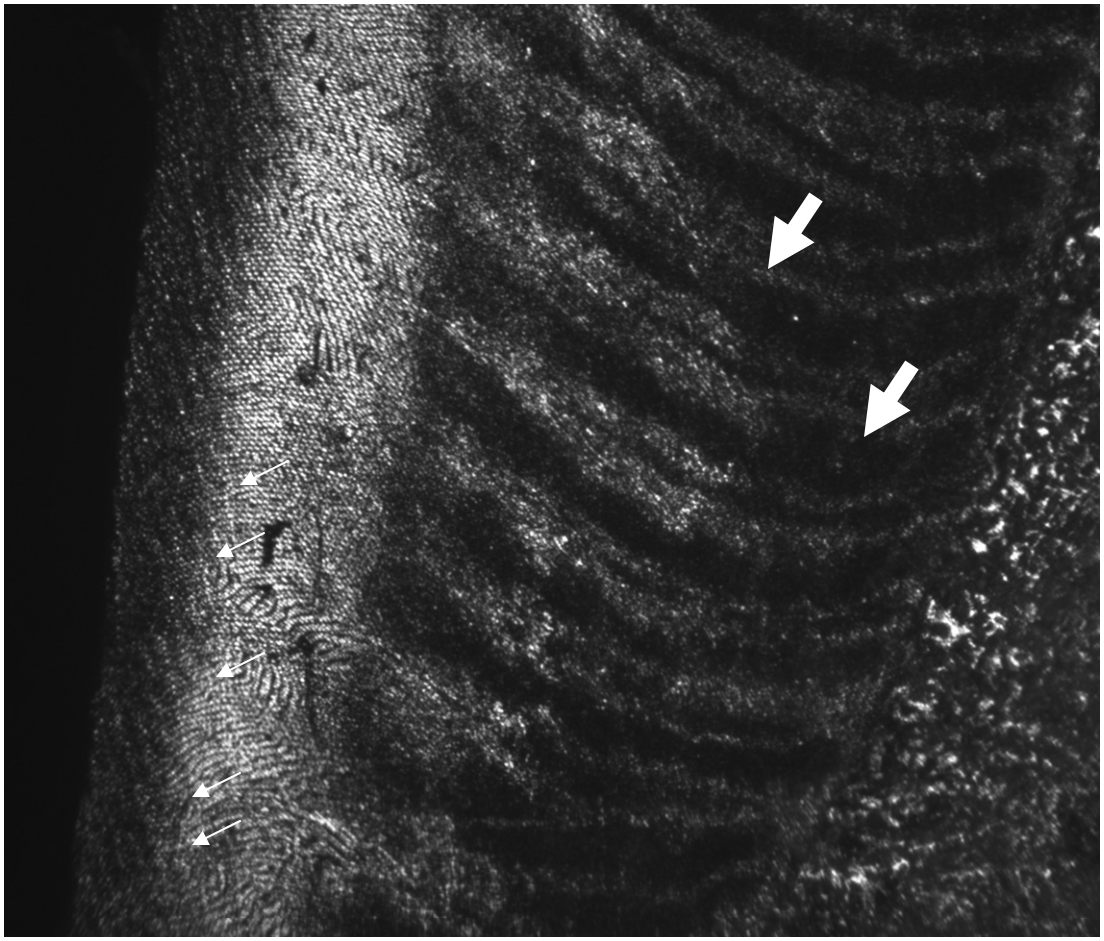

Figure 3(2).10. Image of Stw 402, an M^1 attributed to *A. africanus*. The specimen was imaged without applying clearing medium. White bold arrows = HSB; small white arrows = striae of Retzius. 5x lens and 0.5 adapter. FW 3.5 mm. CF 1.

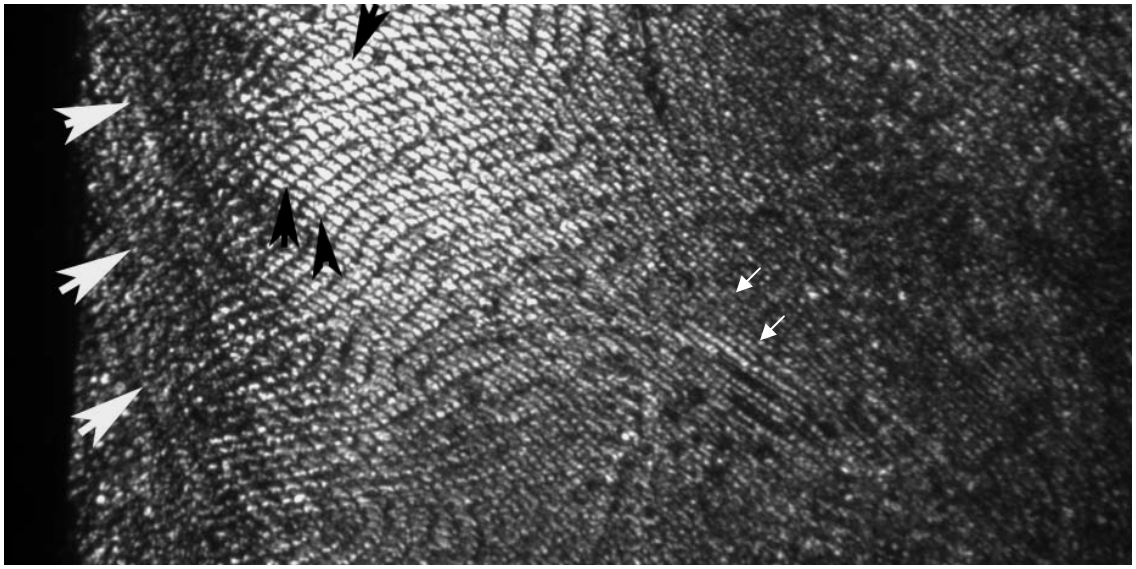

Figure 3 (2).11. Stw 402 using 5x lens and 1:1 adapter. Bold white arrows = striae of Retzius. Black arrows indicate prisms fractured end-on, not cross striations. Cross striations can be seen on the right side of the image indicated by thin white arrows. FW 950 μm. CF1.

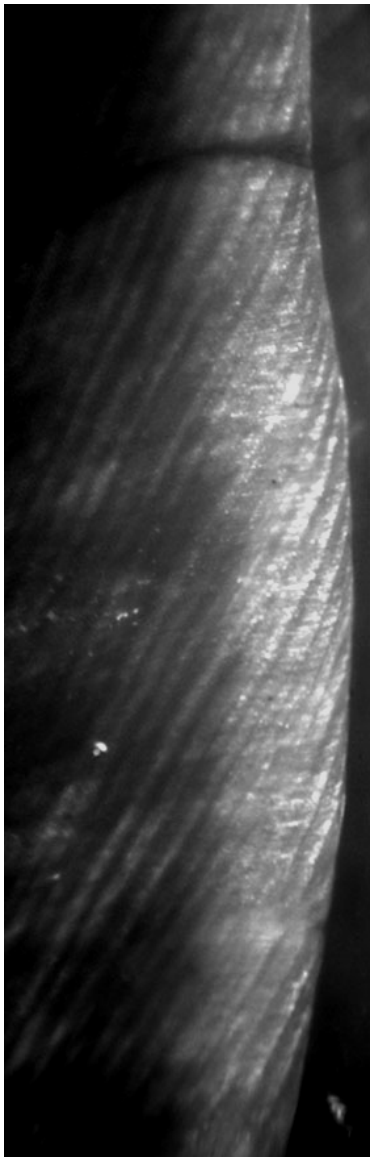

Figure 3(2). 12. Stw 284 an *A. africanus* molar in which striae can be easily observed near the enamel surface using 10x lens, 1:1 adapter. Immersion oil was applied to the surface and a cover slip was placed over the medium, avoiding high reflection from the surface. FW 330 μm. CF1.

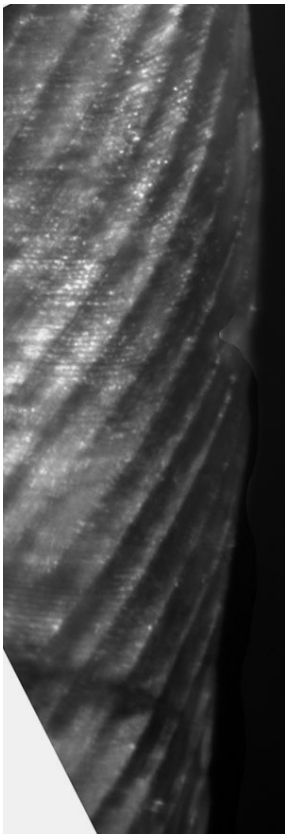

Figure 3(2). 13. Specimen SK 35 (*P. robustus*) from Swartkrans in which striae can be observed using immersion oil on the surface. 10x lens was used with 1: 1 adapter. No cover slip was used in this instance. FW 245 µm. CF 1.

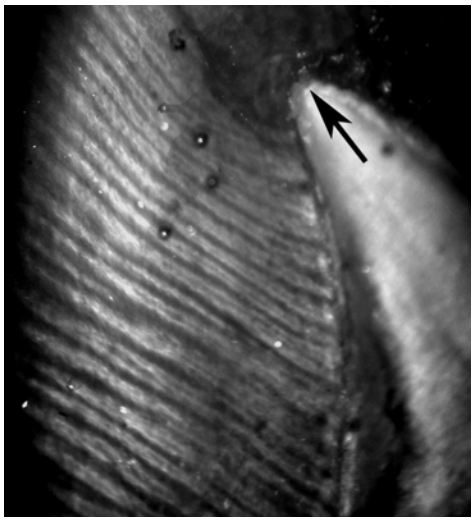

Figure 3(2).14. Specimen SKX 268 originally attributed to *Homo* (Grine 1993). However, the shape of the HSB is more similar to *Paranthropus*. Macho & Thackeray (1992) noted differences in enamel thickness between SK 268 and the remaining *Paranthropus* sample from Swartkrans, being less thick in this specimen. The arrow marks the position of the apparent dentine horn. Immersion oil was used in this specimen with the 5x lens and 0.5 adapter. No cover slip was used. Tiny air bubbles are noticeable in this image. FW 2.2 mm. CF 1.

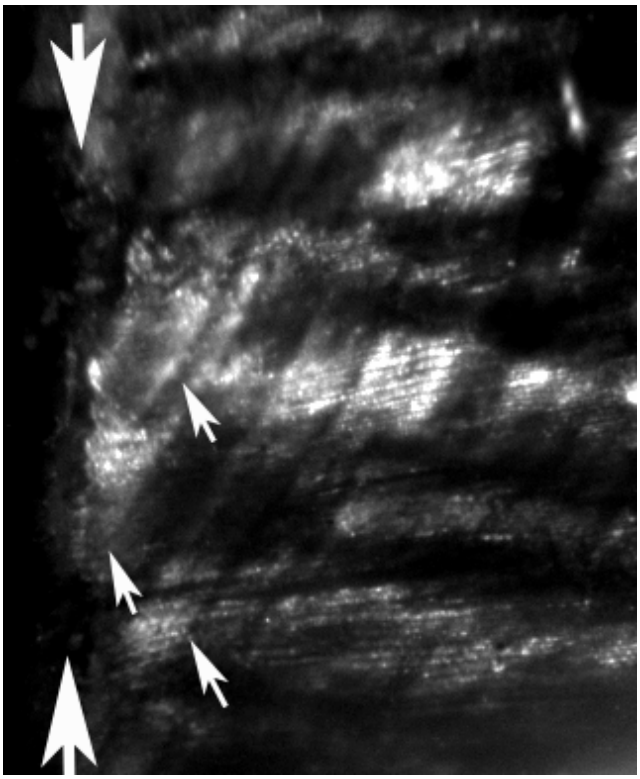

Figure 3(2).15. Stw 90, *A. africanus* molar in which angles formed between the striae (small white arrows) and the EDJ (two larger white arrows) are evident**.** FW 120 μm. CF2.

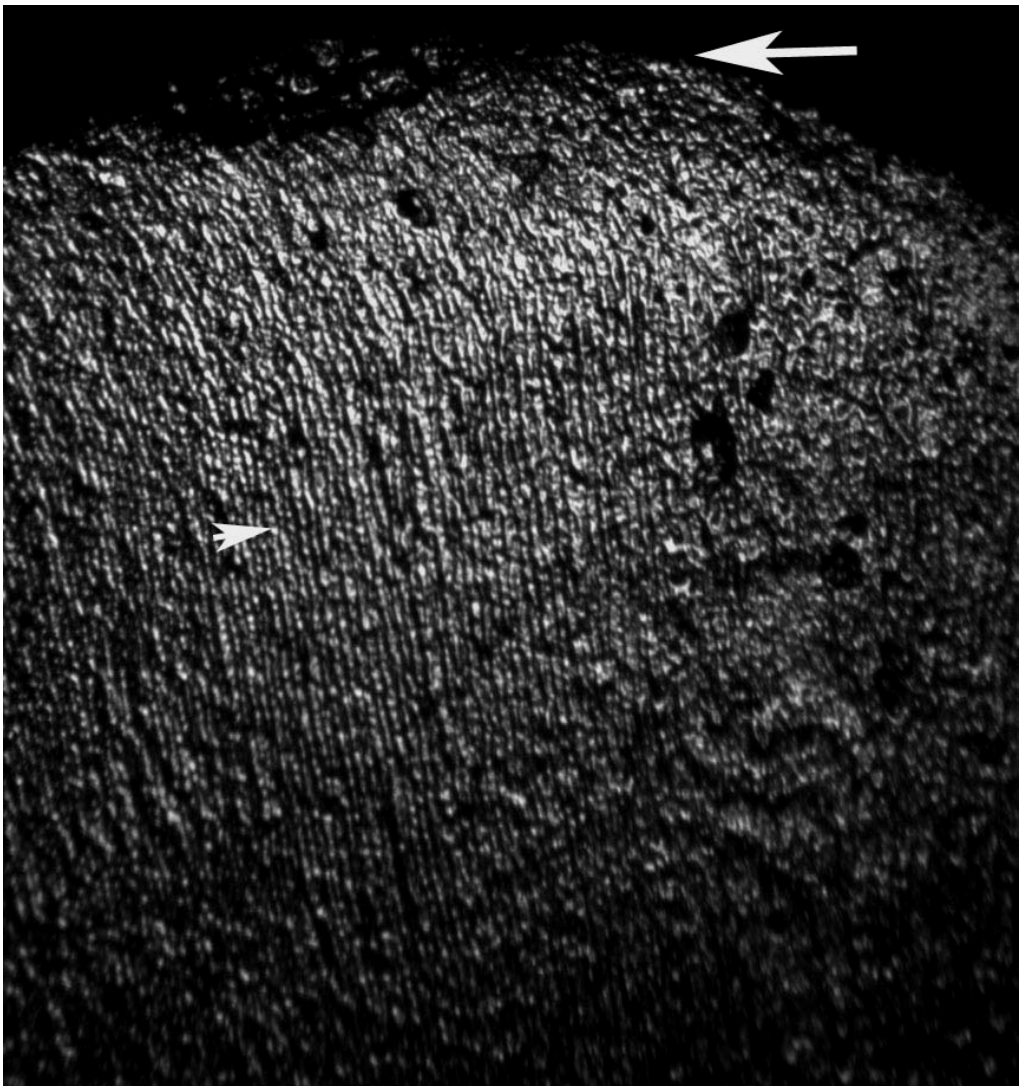

Figure 3(2).16. Cusp of the protocone of STW 284 imaged using 10x lens and 1:1 adapter. Prisms can be seen running almost vertically, and cross striations (one marked with a white arrow) can be seen along the prisms in many places. No clearing medium was used. Top arrow indicates tip of crown. FW 1.4 mm. CF1.

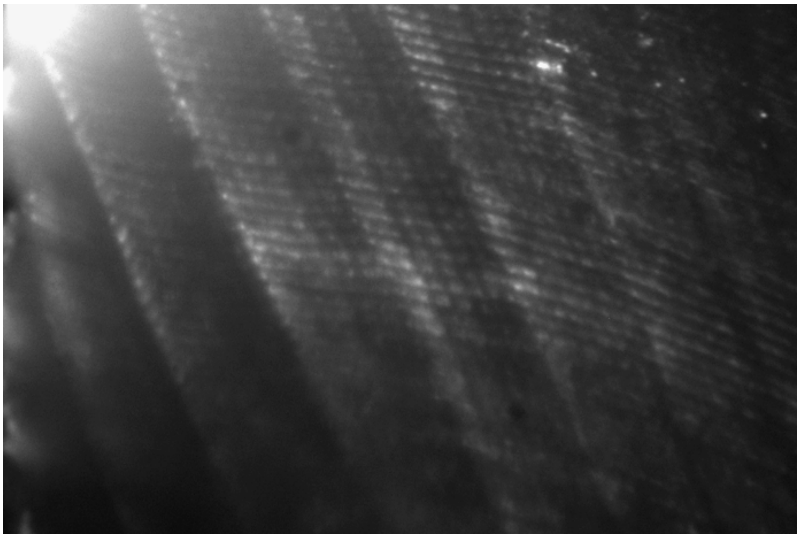

Figure 3(2).17. Swartkrans specimen SK 875. This image was taken using 20x lens and 1:1 adapter after placing some drops of clearing medium over the specimen. This image was taken at the boundary between lateral and cervical enamel on the outer enamel surface. The bright spot on the top left corner is a reflection from the clearing medium. Striae, prisms and cross striations can be observed in this image (see Figure 3(2). 20). FW 380 µm. CF 1.

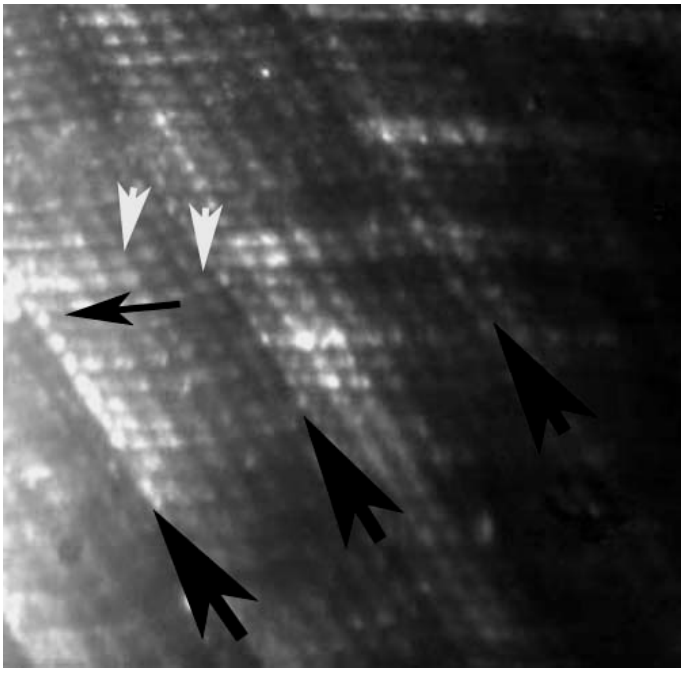

Figure 3(2). 18. Detail of Figure 3 (2) 17. Striae are marked with bold black arrows. Cross striations are marked with white arrows and the small black horizontal arrow indicates prism direction. FW 190 µm. CF 1.

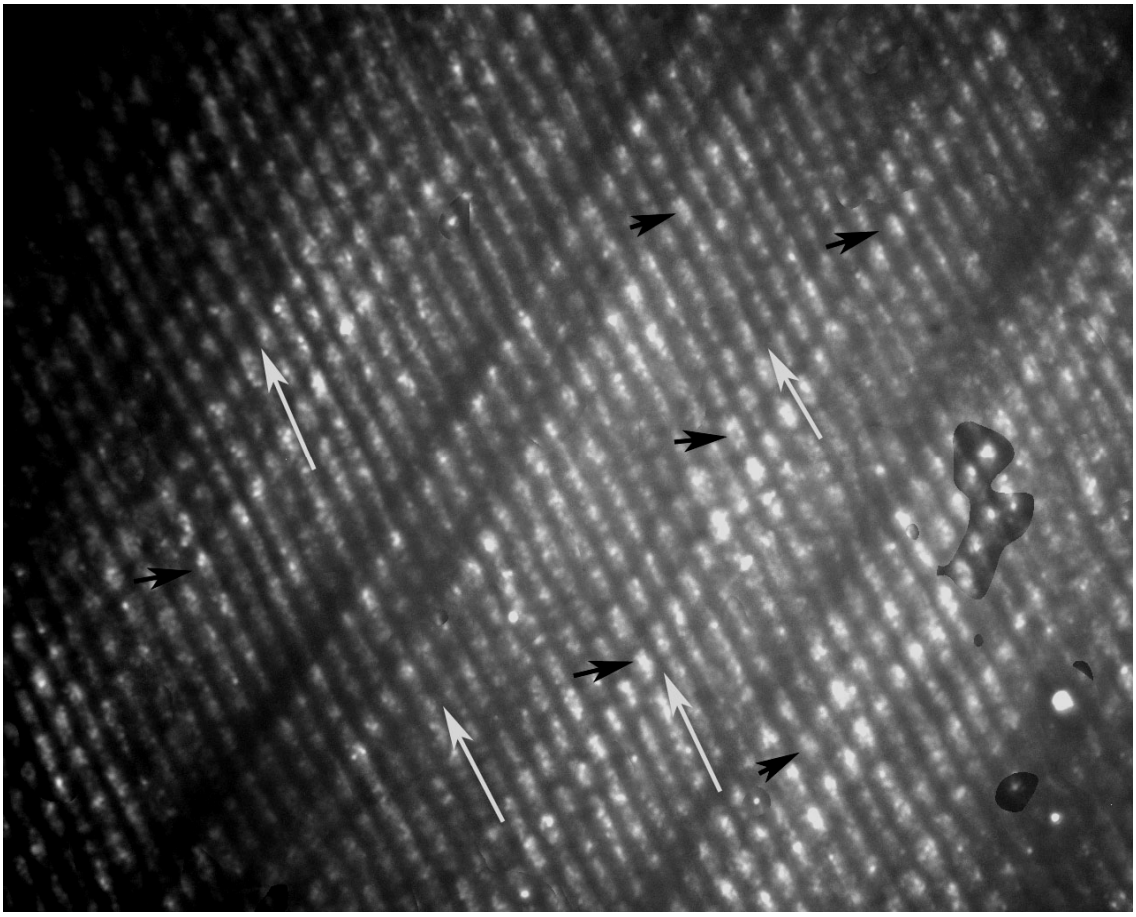

Figure 3(2). 19. Cross striations (varicosities along the prism) shown in mid-cuspal enamel of an *A. africanus* molar. White arrows indicate the prism direction and also interprismatic enamel. Black arrows indicate individual cross striations. Splotches at lower right are artifacts of montaging. Image taken with 50x lens and 1:1 adapter using a clearing medium with no cover slip. FW 190 µm. CF 2.

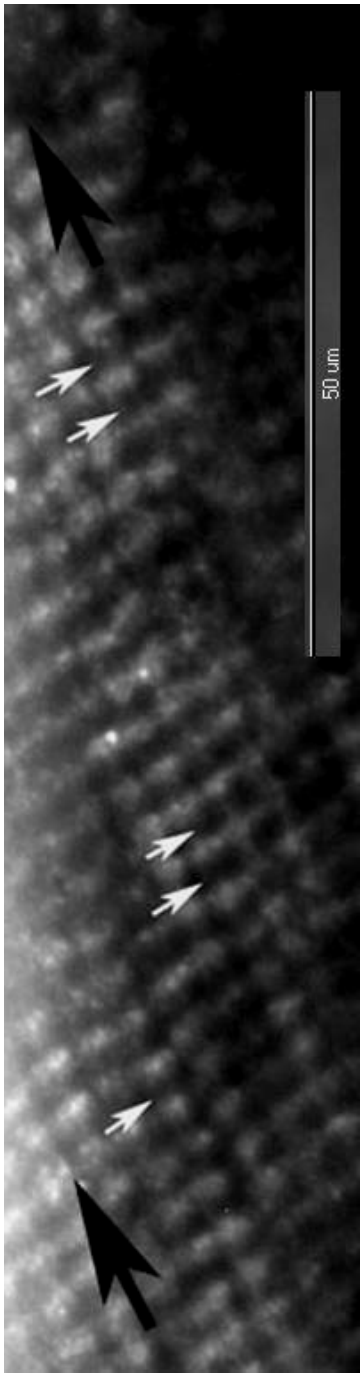

Figure 3(2). 20. Cross striations (white arrows) on the broken surface of a *P. robustus* molar imaged using 50x and 1:1 adapter in the outer cervical enamel. Large black arrows indicate prism direction. Scale 50 microns.

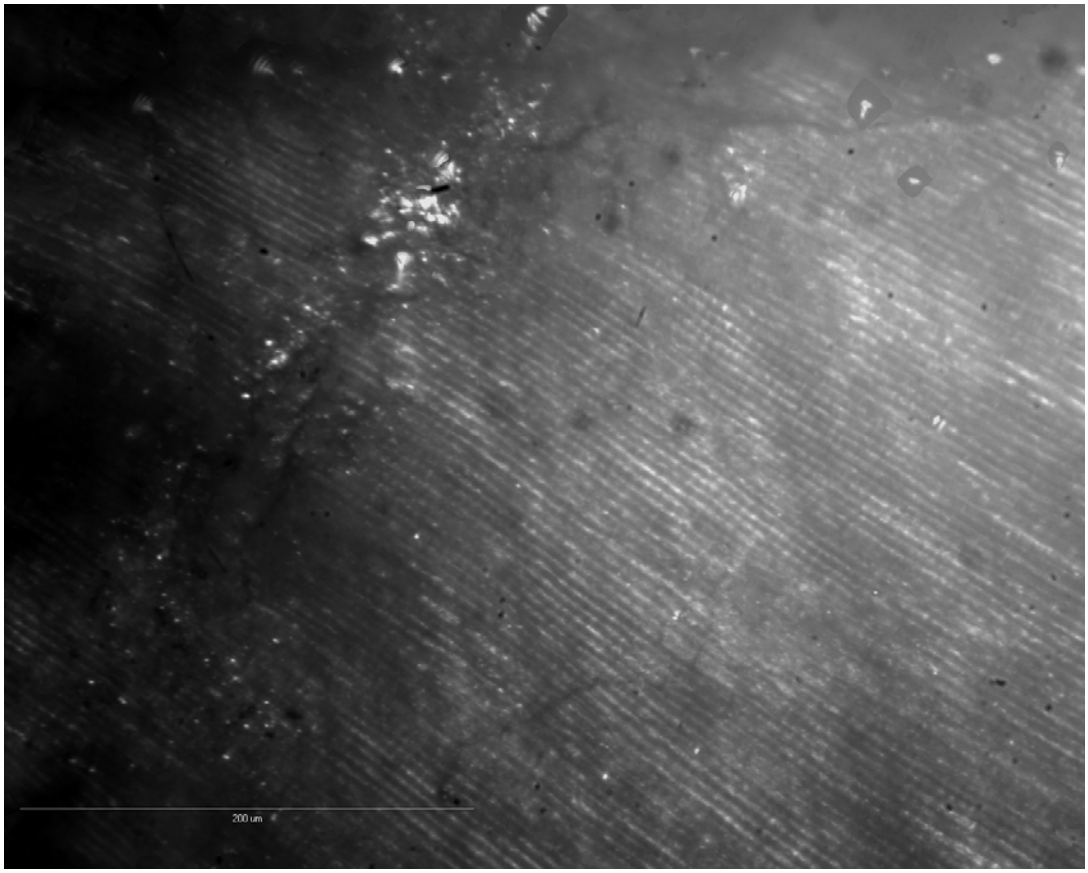

3 (2). 21. Prisms imaged on a natural fracture in a Pliocene hominid molar (AL 366, not included in this study). Prisms are running in an oblique direction from the top left to the bottom right part of the image. Unusually in this instance, prisms could be imaged on a straight course for over 400 microns. Cross striations can be easily observed on the centre and right side of the image. A 20x lens and 1:1 adapter were used. Scale is 200 microns. CF 1.

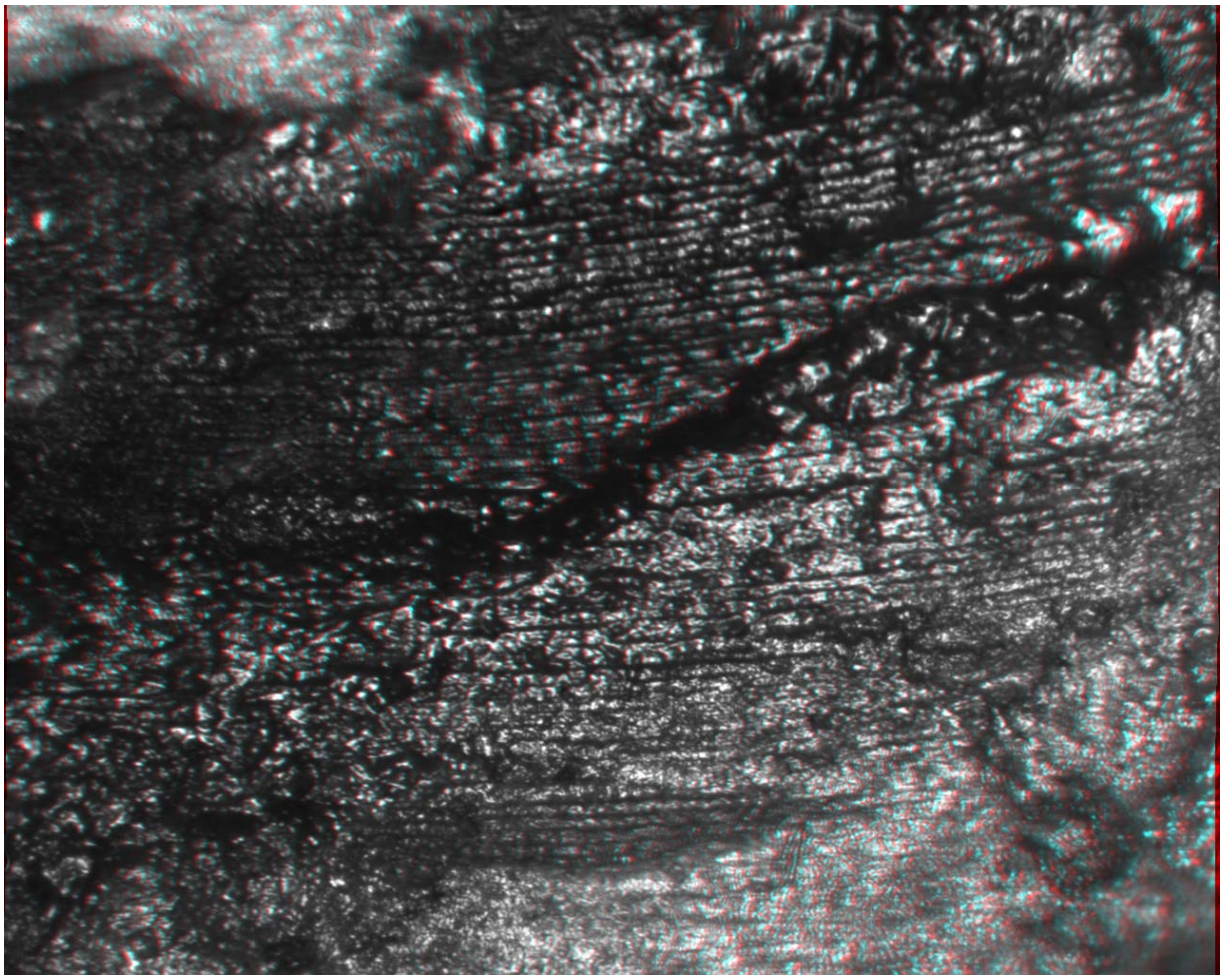

Figure 3 (2). 22. Analglyph 3-D image taken with the PCSOM and using Syncroscopy AutoMontage software (red/cyan glasses are required to visualize the 3D)**.** This image was taken on a natural break occurring on the enamel of a fossil hominid showing the topography of the surface studied. In most cases, without such image capture software, the relief in natural fractures would make it difficult to image enamel prisms at high magnification for any great length as prisms tend to disappear and there are drops of a few hundred microns between adjacent points. In the image, enamel prisms can be seen running from left to right.

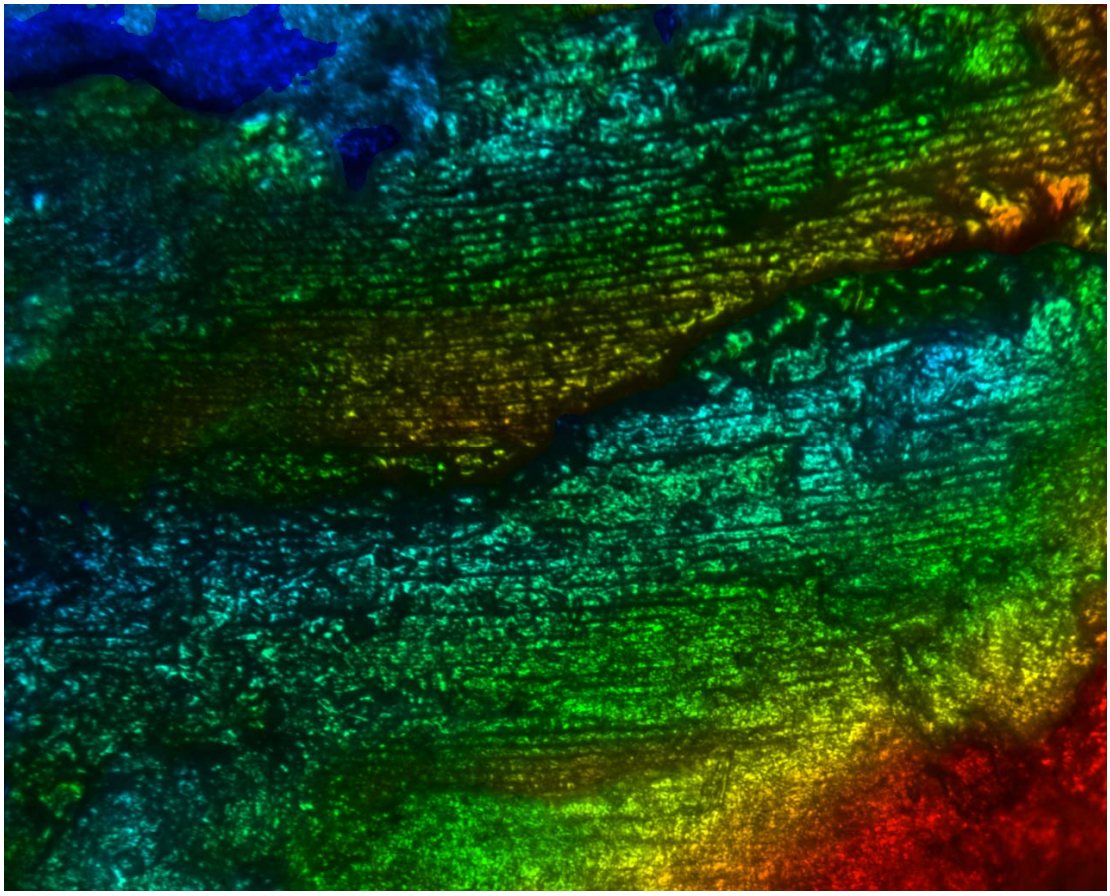

Figure 3 (2). 23. Same specimen as in Figure 3 (2) 25 but here is shown a Syncroscopy AutoMontage color depth map. The highest areas are coded in red and the lowest in blue.

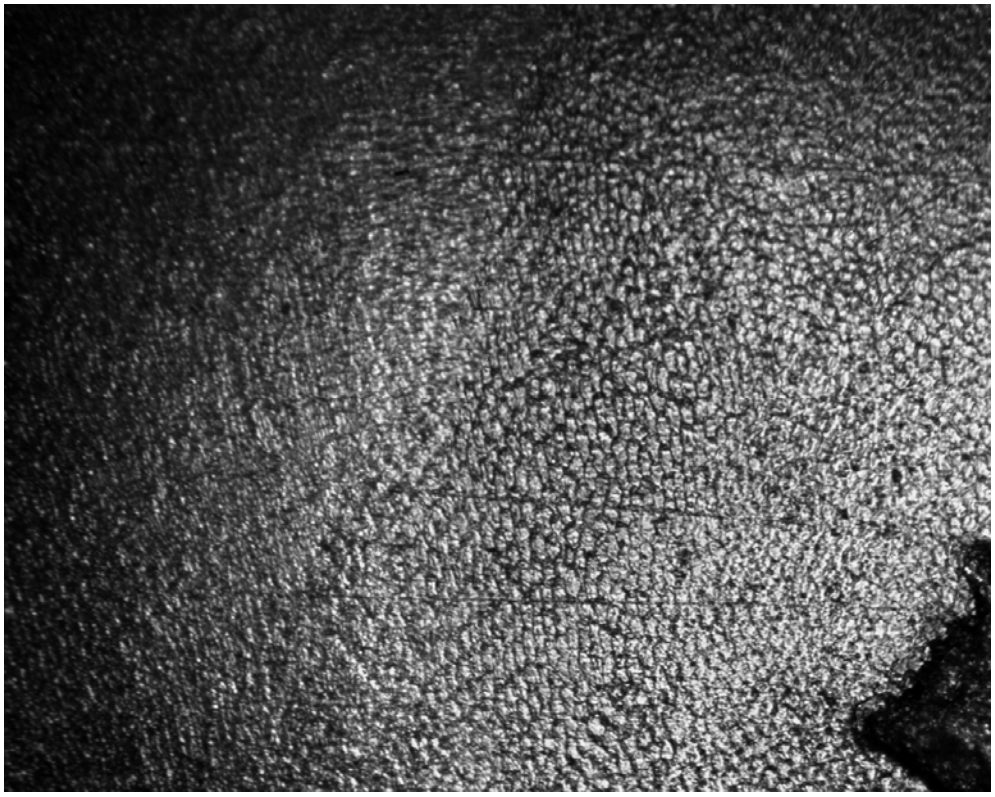

Figure 3 (2). 24. Image of the outer cuspal area of a Pliocene hominid (OMO 398-847, not included in this study) showing prisms running horizontally (left) and diazones to the right of the image. It is interesting to note the localized nature of this decussation very close to the outer cuspal enamel. This specimen was imaged dry using a 50x lens and 0.5 adapter. FW. 280 µ. CF 1.

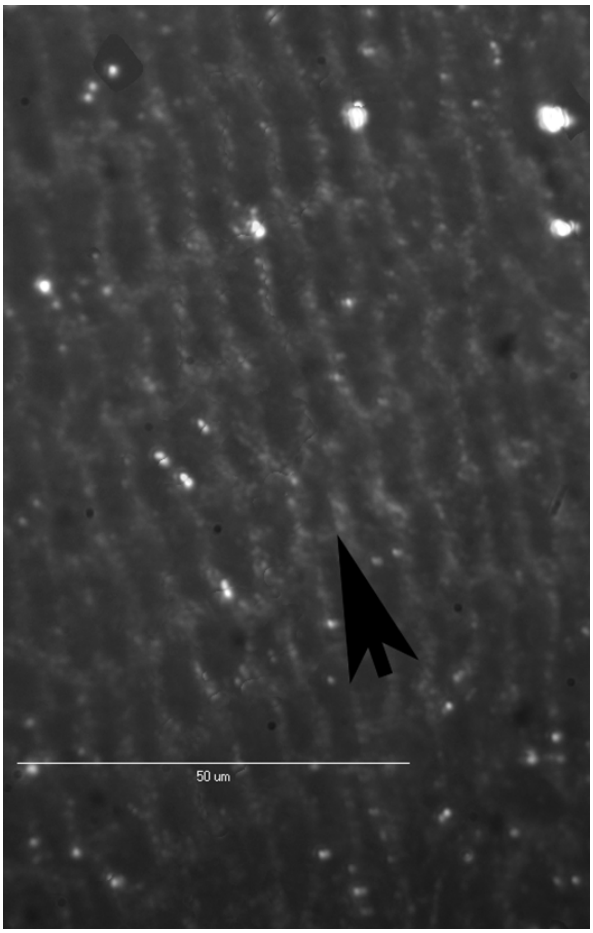

Figure 3 (2) 25. Same specimen as in Figure 3 (2).28 imaged using a clearing medium and cover slip with 50x lens and 1:1 adapter. Scale 50 microns. Black arrow points in prism direction. Decussation is so marked that prisms appear to form the key-hole shape pattern described by Boyde (1964).

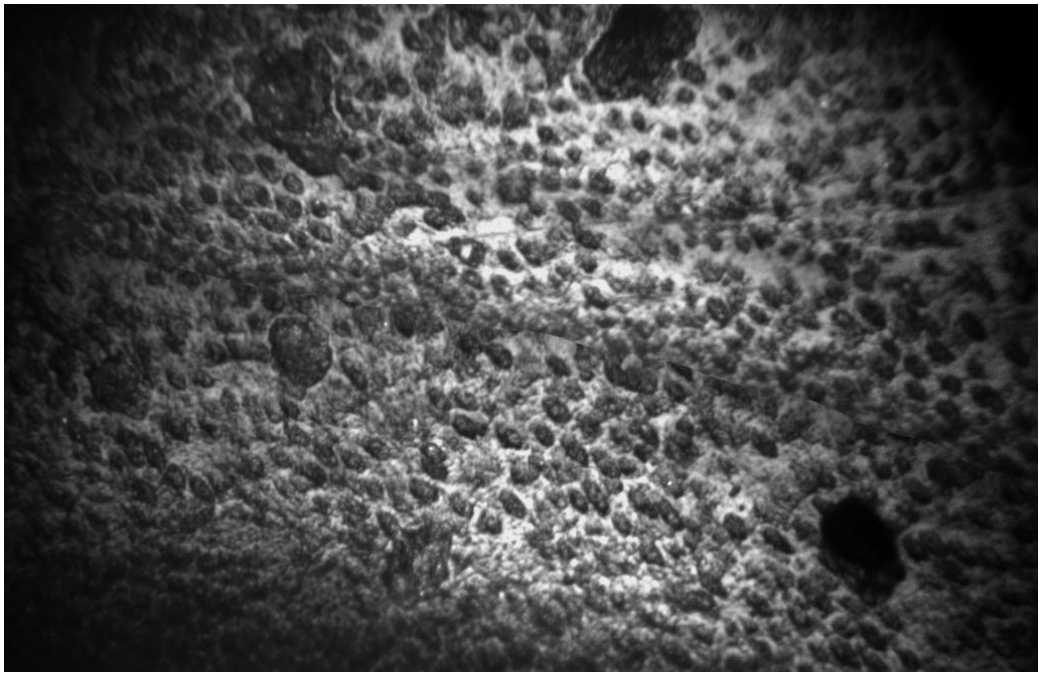

Figure 3(2). 26. Dentine near the cervix of an *A. africanus* molar (Stw 284). No clearing medium was applied. FW 156 µm. CF 2.

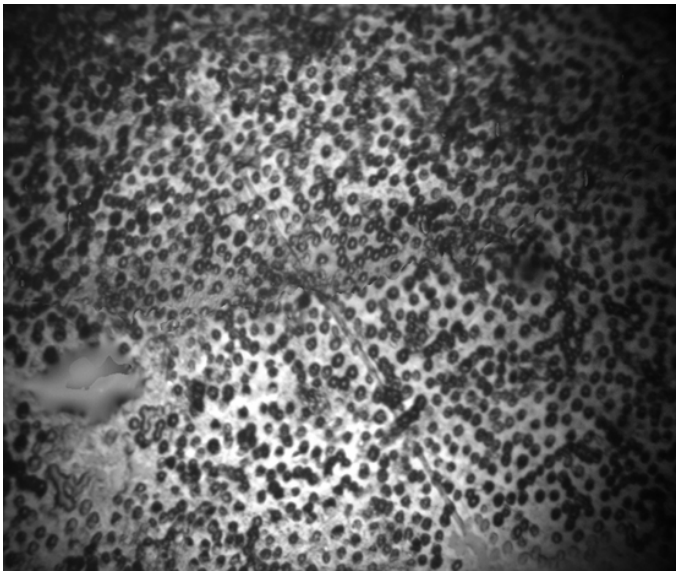

Figure 3(2).27. Dentine in the root of an *A. africanus* molar (Stw 284). No clearing medium was applied. FW 84 µm. CF 1**.**